Quasi-3D Vibrational Analyses of Laminates and Sandwich Plates Resting on Elastic Foundations

A. M. Zenkour
Department of Mathematics, Faculty of Science, King Abdulaziz University, P.O. Box 80203, Jeddah 21589, Saudi Arabia.
Department of Mathematics, Faculty of Science, Kafrelsheikh University, Kafrelsheikh 33516, Egypt.
E-mail: zenkour@gmail.com

D. S. Mashat
Department of Mathematics, Faculty of Science, King Abdulaziz University, P.O. Box 80203, Jeddah 21589, Saudi Arabia.

(Received 5 March 2022; accepted 7 May 2022)

This article establishes the vibrational response of laminates and sandwich plates inserted in an elastic medium. The quasi-3D elasticity equations are used for this purpose. The two-parameter Pasternak's model is utilized to give the interaction between the elastic foundation and the presented plate. The virtual displacement principle is applied to obtain governing dynamic equations. Many validation examples are displayed to show the accuracy and efficiency of the current model. The effects of various parameters like lamination scheme, material properties, aspect and thickness ratios, number of layers, and elastic foundation parameters on vibrations of laminates and sandwich plates are investigated.

1. INTRODUCTION

Numerous research works dealing with the vibrational problem of composite plates and laminates can be observed in the literature. Such studies are done utilizing both numerical and analytical approaches. Here, we restrict our attention to the vibration frequencies of plates lying on elastic foundations. The impacts of foundation parameters on the vibrational responses of composite plates have not had enough attention in the literature.

Three-dimensional (3D) investigation of plates has for some time been an objective for the individuals who work in this field. Such an examination gives sensible outcomes as well as permits further actual experiences, which cannot, in any case, be anticipated by the 2D investigation. Within a thirty year period, a few endeavors have been created for 3D vibration examination of thick plates. However, the majority of them concentrated on rectangular plates.

Two-dimensional theories diminish the elements of issues from three to two by presenting a few concerns in mathematical modeling. This outcome has somewhat straightforward articulations and induction of solutions. These disentanglements inherently achieve errors, and hence improved speculations should not ignore specific modes for thicker plates.

A review of the literature found that Bhattacharya[1] presented the vibrations of cross-ply laminated plates lying on an elastic foundation. Lal et al.[2] studied the effect of foundation parameters on the free vibration of laminates lying on an elastic foundation. Ayvaz and Oguzhan[3] presented frequency parameters of plates laying on elastic foundations employing a revised Vlasov model. Pirbodaghi et al.[4] explored the vibrational study of thin multilayered plates resting on elastic foundations. Akgöz and Civalek[5] offered free vibration of thin laminates lying on elastic foundations. Nedri et al.[6] presented the free vibration of multilayered composite plates lying on elastic foundations utilizing a developed hyperbolic shear deformation theory. Akgöz and Civalek[7] presented the thermo-mechanical size-dependent buckling analysis of embedded FG microbeams. Mercan et al.[8] presented the free vibration behavior of FG circular cylindrical shells. Akgöz and Civalek[9] discussed the static bending behavior of single-walled carbon nanotubes embedded in an elastic medium. Haciyev et al.[10,11] presented the vibration of bi-directional exponentially graded orthotropic and inhomogeneous with spatial coordinates plates resting on the two-parameter elastic or inhomogeneous viscoelastic foundation. Ozdemir[12] studied the vibrational analysis of thick plates resting on Winkler's foundation based upon Mindlin's theory. Rahmani et al.[13] studied the vibration of anti-symmetric laminates lying on viscoelastic foundations in a thermal environment. Mahmure et al.[14] discussed the free vibration of thin-walled composite shells reinforced with carbon nanotubes resting on a two-parameter foundation. Gohari et al.[15] developed an analytical solution for the electro-mechanical flexural response of smart laminated piezoelectric composite rectangular plates. Gohari et al.[16] discussed a new analytical flexural solution for thick multi-layered composite hybrid rectangular plates resting on Winkler elastic foundation. Yang et al.[17] discussed the free vibration and impact response of composite plates with interfacial delamination based on the improved layerwise theory with finite element implementation. Guo et al.[18] presented the free vibration analysis of delaminated composite plates resting on an elastic foundation. Huang et al.[19] investigated the delamination impact on the nonlinear vibrational study of the composite plate lying on an elastic foundation. Avey et al.[20] presented the solution of nonlinear free vibration of composite shells reinforced with carbon nanotubes and resting on elastic soils.

In this paper, an established quasi-3D laminated plate the-

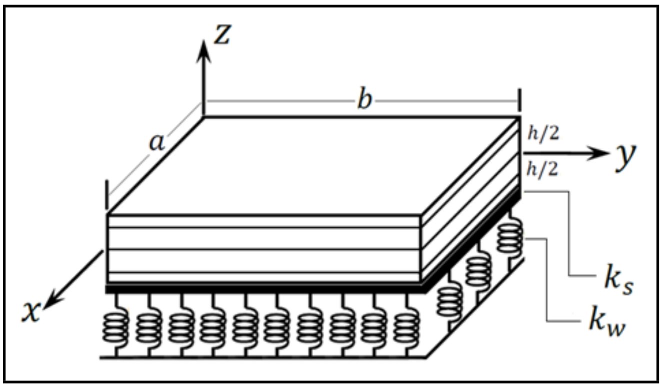

Figure 1. Schematic diagram for the geometry of the laminated plate resting on a two-parameter elastic foundation.

ory is implemented for the vibration of symmetric and anti-symmetric fiber-reinforced laminates and composite plates lying on elastic foundations. It should be mentioned that such a refined theory takes into account that no hypothesis would be created in the progress of the formulas. Numerical results for different lamination schemes are described. Comparisons are done with outcomes available from other assets wherever possible. The analysis is employed to examine the effects of thickness and aspect ratios and elastic foundation factors on the frequency parameters of isotropic and cross-ply laminated plates. Numerical outcomes are illustrated explicitly.

2. BASIC EQUATIONS

Consider a multilayered rectangular plate constrained by the coordinate planes $x_1 = 0, a$, $x_2 = 0, b$, and $x_3 = -h/2, h/2$. The plate is composed of a finite number L of homogeneous layers and laid on a two-parameter Pasternak's elastic foundation. The above cartesian coordinates x_α ($\alpha = 1, 2$), x_3 are chosen such as x_3 is placed on the mid-plane of the plate. The plate is symmetrically/anti-symmetrically disposed of concerning the middle plane (see Fig. 1). The layers are believed completely confined. The material of each element layer is linearly elastic and orthotropic and the layers are described by the same geometrical and physicomechanical properties.

2.1. A Quasi 3D Theory

Let $v_\alpha(x_\alpha, x_3; t)$ and $v_3(x_\alpha, x_3; t)$ indicate the dynamic displacements of a material point located at (x_α, x_3) and time t in the x_1, x_2, and x_3 directions, respectively. It is clear that the Greek lower case subscripts are supposed to range over the integers $1, 2$.

The in-plane displacements and transverse displacement are assumed according to the following refined quasi-3D plate theory:

$$\begin{aligned} v_\alpha &= u_\alpha - x_3 u_{3,\alpha} + \phi(x_3)\psi_\alpha; \\ v_3 &= u_3 + \phi'(x_3)\psi_3; \end{aligned} \tag{1}$$

where the above displacements contain six unknowns u_j and ψ_j as functions on $(x_\alpha; t)$. The effects due to transverse shear strain and normal deformations are both included. The function $\phi(x_3)$ should be an odd function of x_3 while its derivative with respect to x_3 should be an even function of x_3. In fact, there are many forms of the function $\phi(x_3)$ that satisfy the above conditions, these are:

Reddy:[21] $z\left(1 - \frac{4x_3^2}{3h^2}\right)$;
Touratier,[22] Zenkour:[23,24] $\frac{h}{\pi}\sin\left(\frac{\pi x_3}{h}\right)$;
Soldatos:[25] $h\sinh\left(\frac{x_3}{h}\right) - x_3\cosh\left(\frac{1}{2}\right)$;
Karama et al.:[26] $x_3 e^{-2\left(\frac{x_3}{h}\right)^2}$.

In addition to the above forms, there are many others in the literature. Most of them are sufficient to obtain accurate outcomes. In the present model, we restrict our attention to the following effective and sufficient form. That is:

$$\phi(x_3) = \frac{h}{\pi}\sin\left(\frac{\pi x_3}{h}\right); \qquad (\,)' = \frac{d(\,)}{dx_3}. \tag{2}$$

No transversal shear correction factors are needed for the present model because a correct representation of the transversal shearing strain is given. The displacement field in Eq. (1) gives the strains as:

$$\begin{aligned} \begin{Bmatrix} \varepsilon_\alpha \\ \gamma_{12} \end{Bmatrix} &= \begin{Bmatrix} \varepsilon_\alpha^0 \\ \gamma_{12}^0 \end{Bmatrix} + x_3 \begin{Bmatrix} \varepsilon_\alpha^1 \\ \gamma_{12}^1 \end{Bmatrix} + \phi(x_3) \begin{Bmatrix} \varepsilon_\alpha^2 \\ \gamma_{12}^2 \end{Bmatrix}; \\ \gamma_{\alpha 3} &= \phi'(x_3)\gamma_{\alpha 3}^0; \\ \varepsilon_3 &= \phi''(x_3)\varepsilon_3^0; \end{aligned} \tag{3}$$

where:

$$\begin{aligned} &\varepsilon_\alpha^0 = \frac{\partial u_\alpha}{\partial x_\alpha}; \qquad \varepsilon_\alpha^1 = -\frac{\partial^2 u_3}{\partial x_\alpha^2}; \qquad \varepsilon_\alpha^2 = \frac{\partial \psi_\alpha}{\partial x_\alpha}; \\ &\gamma_{\alpha 3}^0 = \frac{\partial \psi_3}{\partial x_\alpha} + \psi_\alpha; \qquad \varepsilon_3^0 = \psi_3; \qquad \gamma_{12}^0 = \frac{\partial u_2}{\partial x_1} + \frac{\partial u_1}{\partial x_2}; \\ &\gamma_{12}^1 = -2\frac{\partial^2 u_3}{\partial x_1 \partial x_2}; \qquad \gamma_{12}^2 = \frac{\partial \psi_2}{\partial x_1} + \frac{\partial \psi_1}{\partial x_2}. \end{aligned} \tag{4}$$

Also, the load-displacement relation between the plate and the supporting foundations is given according to the two-parameter Pasternak's model by:

$$R = (k_w - k_s \nabla^2) u_3; \tag{5}$$

where R is the foundation reaction per unit area, k_w and k_s are Winkler's and Pasternak's foundation stiffnesses, respectively, and ∇^2 represents Laplace operator. Winkler's model is simply obtained when $k_s = 0$.

2.2. Constitutive Equations

By treating each layer as an individual homogeneous plate, the stress-strain relationships in the plate coordinates for the kth layer are written in the form:

$$\begin{Bmatrix} \sigma_1 \\ \sigma_2 \\ \sigma_3 \\ \tau_{23} \\ \tau_{13} \\ \tau_{12} \end{Bmatrix}^{(k)} = \begin{bmatrix} c_{11} & c_{12} & c_{13} & 0 & 0 & 0 \\ & c_{22} & c_{23} & 0 & 0 & 0 \\ & & c_{33} & 0 & 0 & 0 \\ & & & c_{44} & 0 & 0 \\ & \text{symm.} & & & c_{55} & 0 \\ & & & & & c_{66} \end{bmatrix}^{(k)} \begin{Bmatrix} \varepsilon_1 \\ \varepsilon_2 \\ \varepsilon_3 \\ \gamma_{23} \\ \gamma_{13} \\ \gamma_{12} \end{Bmatrix}; \tag{6}$$

where $c_{ij}^{(k)}$ are the transformed elastic coefficients. If the plate composition is cross-ply, the orthotropic material regarding the old coordinate system under rotation through an angle θ_k

($= 0°$ or $90°$) about the x_3-axis so that the transformation expressions for the stiffnesses c_{ij} become:

$$
\begin{aligned}
c_{11}^{(k)} &= c_{11}\cos^4\theta_k + 2(c_{12}+2c_{66})\sin^2\theta_k\cos^2\theta_k + \\
&\quad c_{22}\sin^4\theta_k; \\
c_{12}^{(k)} &= (c_{11}+c_{22}-4c_{66})\sin^2\theta_k\cos^2\theta_k + \\
&\quad c_{12}(\sin^4\theta_k+\cos^4\theta_k); \\
c_{13}^{(k)} &= c_{13}\cos^2\theta_k + c_{23}\sin^2\theta_k; \\
c_{22}^{(k)} &= c_{11}\sin^4\theta_k + 2(c_{12}+2c_{66})\sin^2\theta_k\cos^2\theta_k + \\
&\quad c_{22}\cos^4\theta_k; \\
c_{23}^{(k)} &= c_{13}\sin^2\theta_k + c_{23}\cos^2\theta_k; \\
c_{33}^{(k)} &= c_{33}; \\
c_{44}^{(k)} &= c_{44}\cos^2\theta_k + c_{55}\sin^2\theta_k; \\
c_{55}^{(k)} &= c_{44}\sin^2\theta_k + c_{55}\cos^2\theta_k; \\
c_{66}^{(k)} &= (c_{11}-2c_{12}+c_{22})\sin^2\theta_k\cos^2\theta_k + \\
&\quad c_{66}(\cos^2\theta_k-\sin^2\theta_k)^2; \qquad (7)
\end{aligned}
$$

where c_{ij} are the stiffness matrix components of the lamina,

$$
\begin{aligned}
c_{11} &= \frac{E_1(1-\nu_{23}\nu_3 2)}{\Delta}; \\
c_{12} &= \frac{E_1(\nu_{21}+\nu_{23}\nu_{31})}{\Delta} = \frac{E_2(\nu_{12}+\nu_{32}\nu_{13})}{\Delta}; \\
c_{13} &= \frac{E_1(\nu_{31}+\nu_{21}\nu_{32})}{\Delta} = \frac{E_3(\nu_{13}+\nu_{12}\nu_{23})}{\Delta}; \\
c_{22} &= \frac{E_2(1-\nu_{13}\nu_{31})}{\Delta}; \\
c_{23} &= \frac{E_2(\nu_{32}+\nu_{12}\nu_{31})}{\Delta} = \frac{E_3(\nu_{23}+\nu_{21}\nu_{13})}{\Delta}; \\
c_{33} &= \frac{E_3(1-\nu_{12}\nu_{21})}{\Delta}; \\
c_{44} &= G_{23}; \\
c_{55} &= G_{13}; \\
c_{66} &= G_{12}; \\
\Delta &= 1-\nu_{12}\nu_{21}-\nu_{31}\nu_{13}-\nu_{23}\nu_{32}-2\nu_{21}\nu_{32}\nu_{13}; \qquad (8)
\end{aligned}
$$

in which E_1, E_2, and E_3 are Young's moduli in x_1, x_2, and x_3 directions, respectively; ν_{ij} are Poisson's ratios, and G_{ij} represent shear moduli. Poisson's ratios and Young's moduli are associated by the communal formulae as $\nu_{ij}E_j = \nu_{ji}E_i$, $i,j = 1,2,3$.

2.3. Stress Resultants

The stress resultants can be obtained by integrating Eq. (6) over the thickness as follows:

$$
\begin{aligned}
&\left\{(N_\alpha, M_\alpha, S_\alpha), (N_{12}, M_{12}, S_{12})\right\} = \\
&\qquad \sum_{k=1}^{L}\int_{x_3^{(k)}}^{x_3^{(k+1)}} (1, x_3, \phi)\left\{\sigma_\alpha^{(k)}, \tau_{12}^{(k)}\right\} dx_3; \\
&S_3 = \sum_{k=1}^{L}\int_{x_3^{(k)}}^{x_3^{(k+1)}} \phi''\sigma_3^{(k)}\, dx_3; \\
&\{Q_1, Q_2\} = \sum_{k=1}^{L}\int_{x_3^{(k)}}^{x_3^{(k+1)}} \phi'\left\{\tau_{13}^{(k)}, \tau_{23}^{(k)}\right\} dx_3. \qquad (9)
\end{aligned}
$$

Using Eqs. (3)–(7) in Eq. (8), the stress resultants (N_1, N_2, N_{12}), moments (M_1, M_2, M_{12}), additional moments (S_1, S_2, S_3, S_{12}), and shear forces (Q_1, Q_2) can be obtained. These expressions are given by:

$$
\begin{aligned}
&\begin{Bmatrix} \mathcal{N} \\ \mathcal{M} \\ \mathcal{S} \\ S_3 \end{Bmatrix} = \begin{bmatrix} \mathcal{B} & \overline{\mathcal{B}} & \overline{\overline{\mathcal{B}}} & \mathcal{H} \\ & \mathcal{D} & \overline{\mathcal{D}} & \overline{\mathcal{H}} \\ & & \overline{\overline{\mathcal{D}}} & \overline{\overline{\mathcal{H}}} \\ \text{symm.} & & & A_{33} \end{bmatrix} \begin{Bmatrix} \mathcal{E}^0 \\ \mathcal{E}^1 \\ \mathcal{E}^2 \\ \varepsilon_3^0 \end{Bmatrix}; \\
&\begin{Bmatrix} Q_2 \\ Q_1 \end{Bmatrix} = \begin{bmatrix} A_{44} & 0 \\ 0 & A_{55} \end{bmatrix} \begin{Bmatrix} \gamma_{23}^0 \\ \gamma_{13}^0 \end{Bmatrix}; \qquad (10)
\end{aligned}
$$

where:

$$
\begin{aligned}
&\mathcal{N} = \begin{Bmatrix} N_1 \\ N_2 \\ N_{12} \end{Bmatrix}; \quad \mathcal{M} = \begin{Bmatrix} M_1 \\ M_2 \\ M_{12} \end{Bmatrix}; \quad \mathcal{S} = \begin{Bmatrix} S_1 \\ S_2 \\ S_{12} \end{Bmatrix}; \\
&\mathcal{E}^0 = \begin{Bmatrix} \varepsilon_1^0 \\ \varepsilon_2^0 \\ \gamma_{12}^0 \end{Bmatrix}; \quad \mathcal{E}^1 = \begin{Bmatrix} \varepsilon_1^1 \\ \varepsilon_2^1 \\ \gamma_{12}^1 \end{Bmatrix}; \quad \mathcal{E}^2 = \begin{Bmatrix} \varepsilon_1^2 \\ \varepsilon_2^2 \\ \gamma_{12}^2 \end{Bmatrix}; \\
&\mathcal{B} = \begin{bmatrix} B_{11} & B_{12} & 0 \\ B_{12} & B_{22} & 0 \\ 0 & 0 & B_{66} \end{bmatrix}; \quad \overline{\mathcal{B}} = \begin{bmatrix} \overline{B}_{11} & \overline{B}_{12} & 0 \\ \overline{B}_{12} & \overline{B}_{22} & 0 \\ 0 & 0 & \overline{B}_{66} \end{bmatrix}; \\
&\overline{\overline{\mathcal{B}}} = \begin{bmatrix} \overline{\overline{B}}_{11} & \overline{\overline{B}}_{12} & 0 \\ \overline{\overline{B}}_{12} & \overline{\overline{B}}_{22} & 0 \\ 0 & 0 & \overline{\overline{B}}_{66} \end{bmatrix}; \quad \mathcal{D} = \begin{bmatrix} D_{11} & D_{12} & 0 \\ D_{12} & D_{22} & 0 \\ 0 & 0 & D_{66} \end{bmatrix}; \\
&\overline{\mathcal{D}} = \begin{bmatrix} \overline{D}_{11} & \overline{D}_{12} & 0 \\ \overline{D}_{12} & \overline{D}_{22} & 0 \\ 0 & 0 & \overline{D}_{66} \end{bmatrix}; \quad \overline{\overline{\mathcal{D}}} = \begin{bmatrix} \overline{\overline{D}}_{11} & \overline{\overline{D}}_{12} & 0 \\ \overline{\overline{D}}_{12} & \overline{\overline{D}}_{22} & 0 \\ 0 & 0 & \overline{\overline{D}}_{66} \end{bmatrix}; \\
&\mathcal{H} = \begin{bmatrix} H_{13} \\ H_{23} \\ 0 \end{bmatrix}; \quad \overline{\mathcal{H}} = \begin{bmatrix} \overline{H}_{13} \\ \overline{H}_{23} \\ 0 \end{bmatrix}; \quad \overline{\overline{\mathcal{H}}} = \begin{bmatrix} \overline{\overline{H}}_{13} \\ \overline{\overline{H}}_{23} \\ 0 \end{bmatrix}; \qquad (11)
\end{aligned}
$$

in which $B_{ij}, \overline{B}_{ij}, \ldots$ etc. are the plate stiffness, defined by:

$$
\begin{aligned}
&\left\{B_{ij}, \overline{B}_{ij}, \overline{\overline{B}}_{ij}\right\} = \sum_{k=1}^{L}\int_{x_3^{(k)}}^{x_3^{(k+1)}} c_{ij}^{(k)}\{1, x_3, \phi\}\, dx_3; \\
&\qquad\qquad i,j = 1,2,6; \\
&\left\{D_{ij}, \overline{D}_{ij}, \overline{\overline{D}}_{ij}\right\} = \sum_{k=1}^{L}\int_{x_3^{(k)}}^{x_3^{(k+1)}} c_{ij}^{(k)}\{x_3^2, x_3\phi, \phi^2\}\, dx_3; \\
&\qquad\qquad i,j = 1,2,6; \\
&\left\{H_{\alpha 3}, \overline{H}_{\alpha 3}, \overline{\overline{H}}_{\alpha 3}\right\} = \sum_{k=1}^{L}\int_{x_3^{(k)}}^{x_3^{(k+1)}} c_{\alpha 3}^{(k)}\phi''\{1, x_3, \phi\}\, dx_3; \\
&\qquad\qquad \alpha = 1,2; \\
&\{A_{33}, A_{pp}\} = \sum_{k=1}^{L}\int_{x_3^{(k)}}^{x_3^{(k+1)}} \left\{c_{33}^{(k)}(\phi'')^2, c_{pp}^{(k)}(\phi')^2\right\} dx_3; \\
&\qquad\qquad p = 4,5. \qquad (12)
\end{aligned}
$$

Hamilton's principle can be written as:

$$
\delta\int_{t_1}^{t_2}(T-U)dt = 0; \qquad (13)
$$

where the first variation of the kinetic energy T is represented as:

$$\delta T = -\iint_{\Omega} \sum_{k=1}^{L} \int_{x_3^{(k)}}^{x_3^{(k+1)}} \rho^{(k)} \ddot{v}_i \delta v_i \, dx_3 \, d\Omega; \tag{14}$$

and U is the total potential energy represented as:

$$\delta U = \iint_{\Omega} \left[\sum_{k=1}^{L} \int_{x_3^{(k)}}^{x_3^{(k+1)}} \left(\sigma_i^{(k)} \delta\varepsilon_i + \tau_{ij}^{(k)} \delta\gamma_{ij} \right) dx_3 + R\delta v_3 \right] d\Omega. \tag{15}$$

Using Eqs. (1), (3), (6), (14), and (15), in Eq. (13) and taking the first variation to obtain the next governing equations combined with the current quasi-3D theory:

$$\begin{aligned}
\delta u_1: \quad & \frac{\partial N_1}{\partial x_1} + \frac{\partial N_{12}}{\partial x_2} = I_0 \ddot{u}_1 - I_1 \frac{\partial \ddot{u}_3}{\partial x_1} + I_3 \ddot{\psi}_1; \\
\delta u_2: \quad & \frac{\partial N_{12}}{\partial x_1} + \frac{\partial N_2}{\partial x_2} = I_0 \ddot{u}_2 - I_1 \frac{\partial \ddot{u}_3}{\partial x_2} + I_3 \ddot{\psi}_2; \\
\delta u_3: \quad & \frac{\partial^2 M_1}{\partial x_1^2} + 2\frac{\partial^2 M_{12}}{\partial x_1 \partial x_2} + \frac{\partial^2 M_2}{\partial x_2^2} - R = \\
& I_0 \ddot{u}_3 + I_1 \left(\frac{\partial \ddot{u}_1}{\partial x_1} + \frac{\partial \ddot{u}_2}{\partial x_2} \right) - I_2 \nabla^2 \ddot{u}_3 + \\
& I_4 \left(\frac{\partial \ddot{\psi}_1}{\partial x_1} + \frac{\partial \ddot{\psi}_2}{\partial x_2} \right) + I_6 \ddot{\psi}_3; \\
\delta \psi_1: \quad & \frac{\partial S_1}{\partial x_1} + \frac{\partial S_{12}}{\partial x_2} - Q_1 = I_3 \ddot{u}_1 - I_4 \frac{\partial \ddot{u}_3}{\partial x_1} + I_5 \ddot{\psi}_1; \\
\delta \psi_2: \quad & \frac{\partial S_{12}}{\partial x_1} + \frac{\partial S_2}{\partial x_2} - Q_2 = I_3 \ddot{u}_2 - I_4 \frac{\partial \ddot{u}_3}{\partial x_2} + I_5 \ddot{\psi}_2; \\
\delta \psi_3: \quad & \frac{\partial Q_1}{\partial x_1} + \frac{\partial Q_2}{\partial x_2} - S_3 = I_6 \ddot{u}_3 + I_7 \ddot{\psi}_3;
\end{aligned} \tag{16}$$

where:

$$\{I_0, I_1, I_2, I_3, I_4, I_5, I_6, I_7\} = \sum_{k=1}^{L} \int_{x_3^{(k)}}^{x_3^{(k+1)}} \rho^{(k)} \left\{1, x_3, x_3^2, \phi, x_3\phi, \phi^2, \phi', (\phi')^2\right\} dx_3. \tag{17}$$

3. SOLUTION PROCEDURE

The current problem connected with the equations of motion of plates lying on elastic foundations, is the exact closed-form solution to Eq. (16), can be composed with the next boundary conditions. The plate is supposed to be simply supported on all four edges. The boundary conditions are required at the side edges for the current quasi-3D plate theory as:

$$\begin{aligned}
& u_2 = u_3 = \phi_2 = \phi_3 = N_1 = M_1 = S_1 = 0, \ \text{ at } \ x_1 = 0, a; \\
& u_1 = u_3 = \phi_1 = \phi_3 = N_2 = M_2 = S_2 = 0, \ \text{ at } \ x_2 = 0, b.
\end{aligned} \tag{18}$$

The following closed-form solution is seen to satisfy all governing equations:

$$\begin{Bmatrix} (u_1, \psi_1) \\ (u_2, \psi_2) \\ (u_3, \psi_3) \end{Bmatrix} = \sum_{m=1}^{\infty} \sum_{n=1}^{\infty} \begin{Bmatrix} (U_{mn}, X_{mn}) \cos(\lambda x_1) \sin(\mu x_2) \\ (V_{mn}, Y_{mn}) \sin(\lambda x_1) \cos(\mu x_2) \\ (W_{mn}, Z_{mn}) \sin(\lambda x_1) \sin(\mu x_2) \end{Bmatrix} e^{-i\omega_{mn} t}; \tag{19}$$

where $\lambda = m\pi/a$ and $\mu = n\pi/b$. Also, m and n represent the mode shapes of vibration and indicate the number of half-waves in x_1- and x_2-directions, respectively.

The governing Eqs. (16) after using Eqs. (19) are reduced to:

$$([K] - \Omega_{mn}[P])\{\Delta\} = \{0\}; \tag{20}$$

where $\{\Delta\} = \{u_1, u_2, u_3, \psi_1, \psi_2, \psi_3\}^T$ and the non-zero elements K_{ij} of the symmetric matrix $[\mathcal{K}]$ and P_{ij} of the symmetric matrix $[\mathcal{P}]$ are defined for antisymmetric cross-ply laminates by:

$$\begin{aligned}
& K_{11} = B_{11}\lambda^2 + B_{66}\mu^2; \quad K_{12} = (B_{12} + B_{66})\lambda\mu; \\
& K_{13} = -\lambda[\overline{B}_{11}\lambda^2 + (\overline{B}_{12} + 2\overline{B}_{66})\mu^2]; \\
& K_{14} = \overline{\overline{B}}_{11}\lambda^2 + \overline{\overline{B}}_{66}\mu^2; \quad K_{15} = K_{24} = (\overline{\overline{B}}_{12} + \overline{\overline{B}}_{66})\lambda\mu; \\
& K_{16} = -H_{13}\lambda; \quad K_{22} = B_{66}\lambda^2 + B_{22}\mu^2; \\
& K_{23} = -\mu[(\overline{B}_{12} + 2\overline{B}_{66})\lambda^2 + \overline{B}_{22}\mu^2]; \\
& K_{25} = \overline{\overline{B}}_{66}\lambda^2 + \overline{\overline{B}}_{22}\mu^2; \quad K_{26} = -H_{23}\mu; \\
& K_{33} = D_{11}\lambda^4 + 2(D_{12} + 2D_{66})\lambda^2\mu^2 + D_{22}\mu^4 + \\
& \qquad k_s(\lambda^2 + \mu^2) + k_w; \\
& K_{34} = -\lambda[\overline{D}_{11}\lambda^2 + (\overline{D}_{12} + 2\overline{D}_{66})\mu^2]; \\
& K_{35} = -\mu[(\overline{D}_{12} + 2\overline{D}_{66})\lambda^2 + \overline{D}_{22}\mu^2]; \\
& K_{36} = \overline{H}_{13}\lambda^2 + \overline{H}_{23}\mu^2; \quad K_{44} = \overline{\overline{B}}_{11}\lambda^2 + \overline{\overline{B}}_{66}\mu^2 + A_{55}; \\
& K_{45} = (\overline{\overline{B}}_{12} + \overline{\overline{B}}_{66})\lambda\mu; \quad K_{46} = (A_{55} - \overline{\overline{H}}_{13})\lambda; \\
& K_{55} = \overline{\overline{B}}_{66}\lambda^2 + \overline{\overline{B}}_{22}\mu^2 + A_{44}; \quad K_{56} = (A_{44} - \overline{\overline{H}}_{23})\lambda; \\
& K_{66} = A_{55}\lambda^2 + A_{44}\mu^2 + A_{33}; \\
& P_{11} = P_{22} = I_0; \quad P_{13} = -I_1\lambda; \quad P_{14} = P_{25} = I_3; \\
& P_{23} = -I_1\mu; \quad P_{33} = I_0 + I_2(\lambda^2 + \mu^2); \quad P_{34} = -I_4\lambda; \\
& P_{35} = -I_4\mu; \quad P_{36} = I_6; \quad P_{44} = P_{55} = I_5; \quad P_{66} = I_7.
\end{aligned} \tag{21}$$

4. NUMERICAL RESULTS AND DISCUSSIONS

The following presents many numerical examples for the vibrational analysis of an isotropic single-layer and cross-ply multi-layer plates. The accuracy and efficiency of the present developed quasi-3D plate theory in calculating various frequencies of simply-supported laminated plates are reviewed. The outcomes included here are compared with those cited in the literature utilizing various theories. Most of the presented examples shown here are for cross-ply multi-layered rectangular plates composed of orthotropic layers. In a particular case,

Table 1. Comparisons of fundamental frequencies $\overline{\omega}_{11} = \omega_{11} h\sqrt{\rho/E_2}$ of cross-ply square plates ($a/h = 5$, Material I).

No. of layers	Source	E_1/E_2			
		10	20	30	40
3	Present	0.326896	0.370288	0.394891	0.411650
	3D Elasticity (Noor[27])	0.32841	0.38241	0.41089	0.43006
	HSDPT (Putcha and Reddy[28])	0.33095	0.38112	0.41094	0.43155
	HSDPT (Khdeir[29])	0.32604	0.36939	0.39390	0.41053
	HSDT (Khdeir and Librescu[30])	0.32711	0.37009	0.39387	0.40962
	FSDT (Khdeir and Librescu[30])	0.32739	0.37110	0.39540	0.41158
	CPT (Khdeir and Librescu[30])	0.42599	0.55793	0.66419	0.75565
5	Present	0.338397	0.394927	0.428708	0.451720
	3D Elasticity (Noor27)	0.34089	0.39792	0.43140	0.45374
	HSDPT (Putcha and Reddy[28])	0.33997	0.39943	0.43509	0.45924
	HSDPT (Khdeir[29])	0.33723	0.39365	0.42143	0.45047
	HSDT (Khdeir and Librescu[30])	0.33741	0.39340	0.42694	0.44986
	FSDT (Khdeir and Librescu[30])	0.33680	0.39306	0.42714	0.45068
	CPT (Khdeir and Librescu[30])	0.42599	0.55793	0.66419	0.75565
9	Present	0.342323	0.403567	0.440728	0.466165
	3D Elasticity (Noor[27])	0.34432	0.40547	0.44210	0.46679
	HSDPT (Putcha and Reddy[28])	0.34220	0.40433	0.44201	0.46769
	HSDPT (Khdeir[29])	0.34125	0.40240	0.43947	0.46480
	HSDT (Khdeir and Librescu[30])	0.34146	0.40202	0.43847	0.46315
	FSDT (Khdeir and Librescu[30])	0.34079	0.40147	0.43818	0.46315
	CPT (Khdeir and Librescu[30])	0.42599	0.55793	0.66419	0.75565

Table 2. Comparisons of the fundamental frequency $\hat{\omega}_{11} = (\omega_{11} b^2/h)\sqrt{\rho/E_2}$ vs. E_1/E_2 of a symmetric $[0°/90°/90°/0°]$ square plate ($a/h = 5$, Material I).

Source	E_1/E_2			
	10	20	30	40
Present	8.29594	9.55074	10.29565	10.81011
3D Elasticity (Noor[27])	8.2103	9.5603	10.272	10.752
HSDPT (Phan and Reddy[31])	8.2718	9.5263	10.272	10.787
HSDPT (Khdeir[29])	8.2718	9.5263	10.272	10.787
HSDT (Khdeir and Librescu[30])	8.2940	9.5439	10.284	10.794
FSDT (Khdeir and Librescu[30])	8.2982	9.5671	10.326	10.854
CPT (Khdeir and Librescu[30])	10.650	13.948	16.605	18.891

Table 3. Comparisons of the fundamental frequency $\hat{\omega}_{11} = (\omega_{11} b^2/h)\sqrt{\rho/E_2}$ vs. a/h of a symmetric $[0°/90°/90°/0°]$ square plate (Material I, $E_1/E_2 = 40$).

Source	a/h								
	2	4	5	10	12.5	20	25	50	100
Present	5.5369	9.3461	10.8101	15.1244	16.1740	17.6542	18.0675	18.6741	18.8370
HSDPT (Wu and Chen[32])	5.317	9.193	10.682	15.069	16.134	17.636	18.055	18.670	18.835
HSDPT (Senthilnarthan et al.[33])	6.002	10.230	11.770	15.940	16.828	17.993	18.301	18.738	18.852
HSDPT (Reddy and Phan[34])	5.576	9.497	10.988	15.270	16.276	17.668	18.050	18.606	18.755
FSDPT (Wu and Chen[32])	5.492	9.369	10.820	15.083	16.120	17.583	18.991	18.590	18.751
CPT (Wu and Chen[32])	15.830	17.907	18.215	18.625	18.707	18.767	18.780	18.799	18.804

however, for comparison with the results obtained in the literature, an isotropic material property has been employed. To check the accuracy and efficiency of the improved solution, and to examine the impacts of transverse shear and normal strains, the next material property sets were applied in achieving the numerical outcomes.

Isotropic plate:

$$E_1/E_2 = 1; \qquad \nu = 0.3. \tag{22}$$

Laminated plate:

Material I:

$$E_1/E_2 = \text{open}; \quad G_{12} = G_{13} = 0.6E_2; \quad G_{23} = 0.5E_2; \\ \nu_{12} = \nu_{13} = \nu_{23} = 0.25. \tag{23}$$

Material II:

$$E_1/E_2 = \text{open}; \quad G_{12} = G_{13} = 0.5E_2; \quad G_{23} = 0.35E_2; \\ \nu_{12} = \nu_{13} = 0.3; \quad \nu_{23} = 0.49. \tag{24}$$

The fundamental and natural frequencies for laminated composite plates are discussed in Tables 1–9 and Figs. 2–18.

Table 1 is devoted to the fundamental frequencies $\overline{\omega}_{11} = \omega_{11} h\sqrt{\rho/E_2}$ of cross-ply square plates ($a/h = 5$, Material I). The outcomes were achieved by employing the present method and are compared with their equivalents found for such theory by applying a finite difference method to the equations of 3D elasticity theory (Noor[27]), frequencies obtained by applying a finite element method (Putcha and Reddy[28]), results using higher-order theory due to Navier solutions (Khdeir[29]), as well as other HSDT, FSDT and CPT reported in (Khdeir and Librescu[30]). An excellent agreement is provided between the presently achieved frequencies and their equivalents available in the literature for different layers of symmetric cross-ply square plates.

Table 4. Comparisons of the fundamental frequency $\hat{\omega}_{11} = (\omega_{11} b^2/h)\sqrt{\rho/E_2}$ of skew-symmetric $[0°/90°/\ldots]$ square plates ($a/h = 5$, Material I).

No. of layers	Source	E_1/E_2				
		3	10	20	30	40
2	Present	6.240408	7.013876	7.852311	8.543846	9.134206
	3D Elasticity (Noor[27])	6.25775	6.98450	7.67450	8.17625	8.56250
	HSDPT (Wu and Chen[32])	6.23199	6.95573	7.64300	8.14264	8.52737
	HSDPT (Putcha and Reddy[28])	6.21689	6.98869	7.82105	8.50504	9.08711
	HSDT (Reddy and Khdeir[35])	6.21689	6.98869	7.82105	8.50504	9.08711
	FSDPT (Wu and Chen[32])	6.20855	6.93924	7.70599	8.32112	8.83331
	CPT (Wu and Chen[32])	6.77050	7.74200	8.85550	9.83375	10.72100
4	Present	6.524282	8.21610	9.641974	10.545819	11.179431
	3D Elasticity (Noor[27])	6.54550	8.14450	9.40550	10.16500	10.67975
	HSDPT (Wu and Chen[32])	6.50437	8.09280	9.34539	10.09988	10.61133
	HSDPT (Putcha and Reddy[28])	6.50081	8.19541	9.62646	10.53478	11.17156
	HSDT (Reddy and Khdeir[35])	6.50081	8.19541	9.62646	10.53478	11.17156
	FSDPT (Wu and Chen[32])	6.50425	8.22460	9.68846	10.61976	11.27077
	CPT (Wu and Chen[32])	7.16900	9.71925	12.47675	14.72500	16.67250

Table 5. Comparisons of fundamental frequencies $\overline{\omega}_{11} = \omega_{11} h\sqrt{\rho/E_2}$ of cross-ply square plates ($a/h = 5$, Material II).

Lamination	No. of layers	Source	E_1/E_2				
			3	10	20	30	40
Skew-symmetric	2	Present	0.23925	0.26877	0.28574	0.32688	0.34879
		Noor and Burton[36]	0.2392	0.2671	0.2815	0.3117	0.3256
		Kant and Kommineni[37]	0.2388	0.2675	0.2809	0.3117	0.3236
		Matsunaga[38]	0.2389	0.2669	0.2812	0.3116	0.3255
	4	Present	0.25036	0.31282	0.34139	0.39326	0.41403
		Noor and Burton[36]	0.2493	0.3063	0.3307	0.3726	0.3887
		Kant and Kommineni[37]	0.2495	0.3002	0.3306	0.3725	0.3899
		Matsunaga[38]	0.2491	0.3063	0.33093	0.3731	0.3893
	6	Present	0.25260	0.32078	0.35113	0.40493	0.42608
		Noor and Burton[36]	0.2517	0.3164	0.3441	0.3914	0.4092
		Kant and Kommineni[37]	0.2517	0.3171	0.3442	0.3918	0.4100
		Matsunaga[38]	0.2519	0.3169	0.3449	0.3926	0.4106
	10	Present	0.23999	0.26427	0.27334	0.26008	0.21173
		Noor and Burton[36]	0.2530	0.3220	0.3518	0.4027	0.4220
		Kant and Kommineni[37]	0.2531	0.3224	0.3519	0.4028	0.4220
		Matsunaga[38]	0.2536	0.3237	0.3542	0.4066	0.4265
Symmetric	3	Present	0.25172	0.30730	0.32821	0.36261	0.37626
		Noor and Burton[36]	0.2516	0.3109	0.3344	0.3739	0.3892
		Matsunaga[38]	0.2513	0.3070	0.3278	0.3616	0.3745
	5	Present	0.25365	0.32081	0.34893	0.39713	0.41573
		Noor and Burton[36]	0.2529	0.3195	0.3470	0.3931	0.4102
		Kant and Kommineni[37]	0.2528	0.3201	0.3470	0.3935	0.4121
		Matsunaga[38]	0.2527	0.3173	0.3437	0.3876	0.4040
	7	Present	0.25405	0.32404	0.35401	0.40590	0.42600
		Noor and Burton[36]	0.2533	0.3222	0.3514	0.4005	0.4190
		Kant and Kommineni[37]	0.2534	0.3224	0.3520	0.4004	0.4204
		Matsunaga[38]	0.2535	0.3218	0.3505	0.3990	0.4173
	9	Present	0.25420	0.32530	0.35599	0.40933	0.43003
		Noor and Burton[36]	0.2535	0.3234	0.3533	0.4040	0.4231
		Kant and Kommineni[37]	0.2536	0.3248	0.3535	0.4047	0.4237
		Matsunaga[38]	0.2540	0.3244	0.3544	0.4058	0.4252

Table 6. Comparisons of fundamental frequencies $\tilde{\omega}_{11} = \omega_{11} a^2\sqrt{\rho h/D}$ of isotropic square plates ($\frac{a}{h} = 20$, $\overline{k}_w = \frac{a^4}{D}k_w$, $\overline{k}_s = \frac{a^2}{D}k_s$).

$\overline{k}_w$	Source	$\overline{k}_s$		
		0	10^2	10^3
0	Lam et al.[39]	19.74	48.62	141.92
	Hasani Baferani and Saidi[40]	19.7374	48.6149	141.8730
	Present	19.60197	48.40897	141.29239
10^2	Lam et al.[39]	22.13	49.63	142.20
	Hasani Baferani and Saidi[40]	22.1261	49.6327	142.2250
	Present	21.98859	49.42342	141.64272
10^3	Lam et al.[39]	37.28	58.00	145.43
	Hasani Baferani and Saidi[40]	37.2763	57.9945	145.3545
	Present	37.10539	57.75690	144.75737

Table 7. Comparisons of fundamental frequencies $\tilde{\omega}_{11} = \omega_{11} a^2 \sqrt{\rho h/D}$ of isotropic square plates ($\bar{k}_w = \frac{a^4}{D} k_w, \bar{k}_s = \frac{a^2}{D} k_s$).

$(\bar{k}_w, \bar{k}_s)$	Source	a/h		
		5	10	10^3
(0,0)	Akhavan et al.[41]	17.5055	19.4260	19.7391
	Thai et al.[42]	17.4523	19.0653	19.7391
	Present	17.56773	19.12477	19.77124
(100,10)	Akhavan et al.[41]	24.3074	25.6368	26.2112
	Thai et al.[42]	24.2722	25.6232	26.2112
	Present	24.07426	25.59158	26.23534
(1000,100)	Akhavan et al.[41]	56.0359	57.3969	57.9961
	Thai et al.[42]	56.0309	57.3921	57.9961
	Present	55.52600	57.03135	58.00701

Table 8. Comparisons of the first three non-dimensional natural frequencies $\tilde{\omega}_{mn} = \frac{\omega_{mn} b^2}{\pi^2} \sqrt{\rho h/D}$ of isotropic square plates ($\bar{k}_w = \frac{a^4}{D} k_w, \bar{k}_s = \frac{a^2}{D} k_s$).

a/h	$\bar{k}_w$	$\bar{k}_s$	Method	Frequencies		
				$\bar{\omega}_{11}$	$\bar{\omega}_{12}$	$\bar{\omega}_{22}$
10	200	0	3D-DQM (Dehghan and Baradaran[43])	2.3903	4.8098	7.2186
			3D-Ritz (Zhou et al.[44])	2.3951	4.8262	7.2338
			FSDPT (Xiang et al.[45])	2.3989	4.8194	7.2093
			HSDPT (Thai et al.[42])	2.3989	4.8198	7.2108
			Present	2.39821	4.83571	7.25056
	1000	0	3D-DQM (Dehghan and Baradaran[43])	3.6978	5.5521	7.7193
			3D-Ritz (Zhou et al.[44])	3.7008	5.5661	7.7335
			FSDPT (Xiang et al.[45])	3.7212	5.5844	7.7353
			HSDPT (Thai et al.[42])	3.7213	5.5847	7.7366
			Present	3.70576	5.57643	7.75071
	200	10	3D-DQM (Dehghan and Baradaran[43])	2.7721	5.2800	7.7132
			3D-Ritz (Zhou et al.[44])	2.7756	5.2954	7.7279
			FSDPT (Xiang et al.[45])	2.7842	5.3043	7.7287
			HSDPT (Thai et al.[42])	2.7842	5.3047	7.7300
			Present	2.77875	5.30496	7.74440
	1000	10	3D-DQM (Dehghan and Baradaran[43])	3.9542	5.9623	8.1816
			3D-Ritz (Zhou et al.[44])	3.9566	5.9757	8.1954
			FSDPT (Xiang et al.[45])	3.9805	6.0078	8.2214
			HSDPT (Thai et al.[42])	3.9805	6.0082	8.2227
			Present	3.96241	5.98746	8.21399
100	100	0	3D-DQM (Dehghan and Baradaran[43])	2.2450	5.1643	8.1338
			3D-Ritz (Zhou et al.[44])	2.2413	5.0973	8.0527
			FSDPT (Xiang et al.[45])	2.2413	5.0971	8.0523
			HSDPT (Thai et al.[42])	2.2413	5.0973	8.0523
			Present	2.24422	5.10525	8.06569
	500	0	3D-DQM (Dehghan and Baradaran[43])	3.0242	5.5474	8.3821
			3D-Ritz (Zhou et al.[44])	3.0214	5.4850	8.3035
			FSDPT (Xiang et al.[45])	3.0215	5.4850	8.3032
			HSDPT (Thai et al.[42])	3.0215	5.4850	8.3032
			Present	3.02352	5.49244	8.31606
	100	10	3D-DQM (Dehghan and Baradaran[43])	2.6578	5.6265	8.6152
			3D-Ritz (Zhou et al.[44])	2.6551	5.5717	8.5406
			FSDPT (Xiang et al.[45])	2.6551	5.5718	8.5405
			HSDPT (Thai et al.[42])	2.6551	5.5718	8.5405
			Present	2.65750	5.57905	8.55285
	500	10	3D-DQM (Dehghan and Baradaran[43])	3.3420	5.9800	8.8500
			3D-Ritz (Zhou et al.[44])	3.3398	5.9285	8.7775
			FSDPT (Xiang et al.[45])	3.3400	5.9287	8.7775
			HSDPT (Thai et al.[42])	3.3400	5.9287	8.7775
			Present	3.34178	5.93541	8.78935

Table 2 is devoted to the fundamental frequencies $\overline{\omega}_{11} = \omega_{11} h \sqrt{\rho/E_2}$ versus E_1/E_2 of a symmetric $[0°/90°/90°/0°]$ square plate ($a/h = 5$). The outcomes achieved by utilizing the present quasi-3D theory are compared with their counterparts in the literature (Noor,[27] Putcha and Reddy,[28] Khdeir,[29] Khdeir and Librescu,[30] Phan and Reddy[31]). Once again, an excellent agreement is retained between the presently achieved frequencies and their counterparts presented in the literature for a four-layer symmetric cross-ply square plate.

The non-dimensional fundamental frequencies $\hat{\omega}_{11} = (\omega_{11} b^2/h)\sqrt{\rho/E_2}$ of a $[0°/90°/90°/0°]$ square plates (Material I, $E_1 = 40E_2$) are considered in Table 3. The dependence of $\hat{\omega}_{11}$ upon the side-to-thickness ratio a/h is discussed. The present results are compared with those obtained in (Wu and Chen[32]) due to local higher-order theory and in (Senthilnarthan et al.;[33] Reddy and Phan[34]) due to global first/higher-order theories. The classical plate theory (CPT) overemphasizes the frequencies while the first-order shear deformation plate theory (FSDPT) underemphasizes them when compared to other higher-order theories. The present global quasi-3D frequencies are favorably compared with those occurring in the literature for different side-to-thickness ratios.

The non-dimensional fundamental frequencies $\hat{\omega}_{11} = (\omega_{11} b^2/h)\sqrt{\rho/E_2}$ of skew-symmetric $[0°/90°/\ldots]$ square plates ($a/h = 5$, Material I) are considered in Table 4. The dependence of the fundamental frequency upon the ratio of

Table 9. Comparisons of the first three non-dimensional natural frequencies $\tilde{\omega}_{mn} = \frac{\omega_{mn} b^2}{\pi^2}\sqrt{\rho h/D}$ of thick square plates ($\overline{k}_s = 10$).

h/b	$\overline{k}_w$	Source	Frequencies $\overline{\omega}_{11}$	$\overline{\omega}_{12}$	$\overline{\omega}_{13}$
0.2	0	Dehghan and Baradaran[43]	2.2275	4.4042	7.2649
		Matsunaga[47]	2.2334	4.4056	7.2436
		Present	2.23983	4.42643	7.29584
	10	Dehghan and Baradaran[43]	2.2481	4.3967	7.2649
		Matsunaga[47]	2.2539	4.4150	7.2488
		Present	2.26058	4.43616	7.30134
	10^2	Dehghan and Baradaran[43]	2.4247	4.4973	7.3161
		Matsunaga[47]	2.4300	4.4986	7.2948
		Present	2.43923	4.52264	7.35059
	10^3	Dehghan and Baradaran[43]	3.7080	5.2276	7.7544
		Matsunaga[47]	3.7112	5.2285	7.7191
		Present	3.77409	5.30046	7.81933
	10^4	Dehghan and Baradaran[43]	4.6065	7.2759	10.0146
		Matsunaga[47]	4.6127	7.2934	10.033
		Present	4.61275	7.29339	10.31442
	10^5	Dehghan and Baradaran[43]	4.6065	7.2760	10.3053
		Matsunaga[47]	4.6127	7.2934	10.314
		Present	4.61275	7.29339	10.31442
0.5	0	Dehghan and Baradaran[43]	1.5913	2.6565	3.8241
		Matsunaga[47]	1.6462	2.6851	3.8268
		Present	1.74351	2.91736	4.12577
	10	Dehghan and Baradaran[43]	1.6055	2.6602	3.8249
		Matsunaga[47]	1.6577	2.6879	3.8274
		Present	1.76180	2.91736	4.12577
	10^2	Dehghan and Baradaran[43]	1.7086	2.6888	3.8316
		Matsunaga[47]	1.7437	2.7096	3.8321
		Present	1.84510	2.91736	4.12577
	10^3	Dehghan and Baradaran[43]	1.8426	2.8000	3.8638
		Matsunaga[47]	1.8451	2.8033	3.8578
		Present	1.84510	2.91736	4.12577
	10^4	Dehghan and Baradaran[43]	1.8426	2.8724	3.8874
		Matsunaga[47]	1.8451	2.8739	3.8866
		Present	1.84510	2.91736	4.12577
	10^5	Dehghan and Baradaran[43]	1.8426	2.8846	3.8902
		Matsunaga[47]	1.8451	2.8857	3.8927
		Present	1.84510	2.91736	4.12577

the elastic modulus to the shear modulus E_1/E_2 is presented. The present outcomes are compared with those obtained in (Noor[27]) due to 3D elasticity and others due to local and global first/higher-order theories (Wu and Chen[32] 1994, Putcha and Reddy,[28] Reddy and Khdeir[35]). It is clear that the frequencies due to the local higher-order theory (Wu and Chen[32] 1994) differ from those of 3D elasticity (Noor[27]) by 0.4% for the range of $E_1/E_2 = 3 - 40$. However, the frequencies due to the global higher-order theories (Putcha and Reddy;[28] Reddy and Khdeir[35]) differ from those of 3D elasticity (Noor[27]) by 0.6% for $E_1/E_2 = 3$ and by 6% for $E_1/E_2 = 40$. It means that the accuracy of the global higher-order theories (Putcha and Reddy;[28] Reddy and Khdeir[35]) becomes poor for highly anisotropic laminates. However, the present global quasi-3D frequencies are favorably compared with those due to 3D elasticity (Noor[27]) and also are more accurate than those due to other global higher-order theories (Putcha and Reddy;[28] Reddy and Khdeir[35]).

Table 5 introduces the comparison of the impact of the number of layers and the degree of orthotropy of individual layers on the fundamental frequency $\overline{\omega}_{11} = \omega_{11} h\sqrt{\rho/E_2}$ of symmetric and skew-symmetric cross-ply laminated plates made of Material II. The degree of orthotropy varied between 3 and 40, and the number of layers varied between 2 and 10. A comparison is created with the 3D solutions reported in Noor and Burton,[36] FEM solutions by Kant and Kommineni,[37] and Navier solutions by Matsunaga.[38] The agreement is generally good. Interestingly, the current frequencies are the most, proposing better accuracy.

Now, to validate the vibration of an isotropic square plate lying on elastic foundations ($a/h = 20$, $\overline{k}_w = a^4 k_w/D$, $\overline{k}_s = a^2 k_s/D$) we present a comparative study of the fundamental frequencies $\tilde{\omega}_{11} = \omega_{11} a^2\sqrt{\rho h/D}$ with the corresponding ones of Lam et al.[39] and Hasani Baferani and Saidi[40] in Table 6. Different values of the elastic foundation parameters are discussed. It is shown that a good agreement between the frequencies is noted. So, the present formulations are reliable for predicting the vibration frequencies of the plate lying on an elastic foundation.

To validate for the thick isotropic plates on an elastic foundation, the nondimensional fundamental frequencies $\tilde{\omega}_{11} = \omega_{11} a^2\sqrt{\rho h/D}$ are compared in Table 7 for thick ($a/h = 5$), moderately-thick ($a/h = 10$), and thin ($a/h = 10^3$) square plates with various values of foundation parameters ($\overline{k}_w, \overline{k}_s$). The calculated nondimensional fundamental frequencies $\overline{\omega}_{11}$ are compared with those reported by Akhavan et al.[41] based on Mindlin's FSDPT and those reported by Thai et al.[42] based on a simple HSDPT. From this table, it is observed that the frequencies of the current theory are in close agreement with those in the literature.

To verify the higher (m, n) modes, the first three non-dimensional frequencies $\tilde{\omega}_{mn} = \frac{\omega_{mn} b^2}{\pi^2}\sqrt{\rho h/D}$ are compared in Table 8 for moderately thick ($a/h = 10$) and thin ($a/h = 100$) square plates with various values of foundation

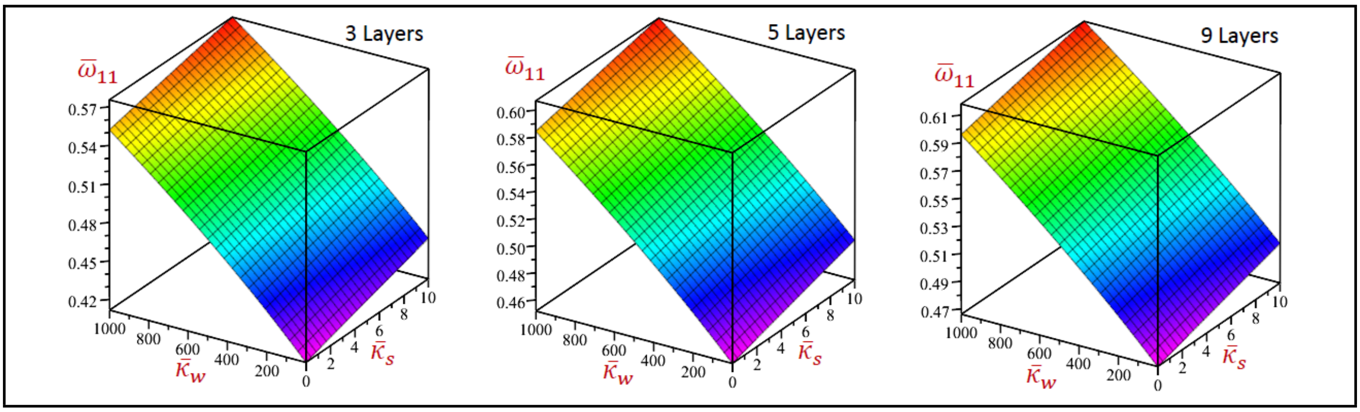

Figure 2. The 3D fundamental frequencies $\overline{\omega}_{11}$ of $(0°/90°/\ldots)$ symmetric square plates vs. Winkler's $\overline{\kappa}_w$, and Pasternak's $\overline{\kappa}_s$ parameters ($a/h = 5$).

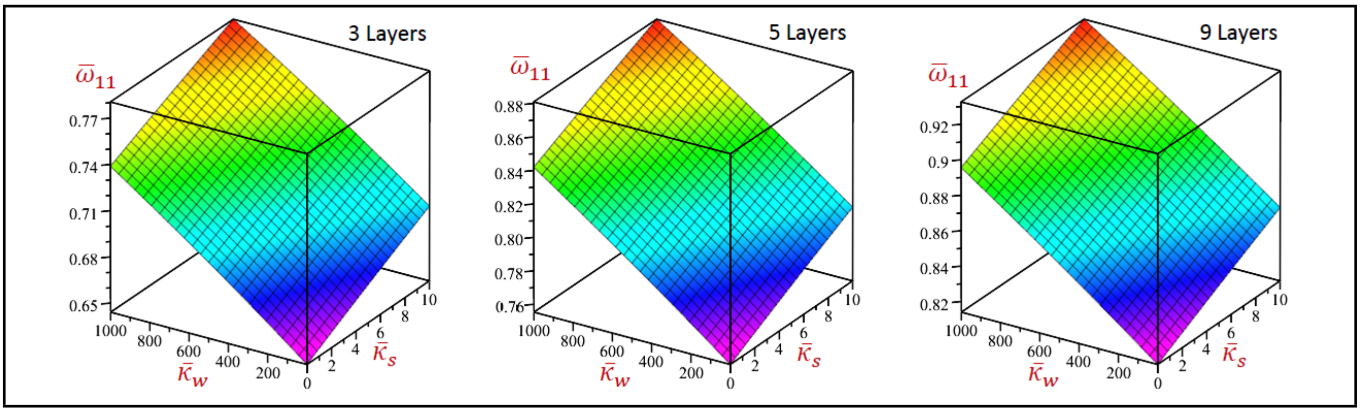

Figure 3. The 3D fundamental frequencies $\overline{\omega}_{11}$ of $(0°/90°/0°/\ldots)$ symmetric rectangular plates vs. Winkler's $\overline{\kappa}_w$, and Pasternak's $\overline{\kappa}_s$ parameters ($a/h = 5$, $a/b = 2$).

parameters $\overline{k}_w$ and $\overline{k}_s$. The present frequencies are compared with the 3D elasticity solutions of Dehghan and Baradaran[43] based on the differential quadrature method and Zhou et al.[44] employing the Ritz method, solutions of Xiang et al.[45] using FSDT as well as a simple HSDPT solution of Thai et al.[42] The results of CPT are also presented by Leissa.[46] The frequencies due to CPT may be suitable for thin plates. It is noticed that the present outcomes are agreeable with other solutions. The frequencies increase with the increase in the mode numbers and the foundation parameters. However, the frequencies decrease as the side-to-thickness ratio increases. The numerical results of the first three non-dimensional natural frequencies $\tilde{\omega}_{mn} = \frac{\omega_{mn} b^2}{\pi^2}\sqrt{\rho h/D}$ for thick isotropic square plates laying on Pasternak foundations ($\overline{k}_s = 10$) are listed in Table 9. The frequencies have been compared with those of Dehghan and Baradaran[43] based on the differential quadrature method and Matsunaga[47] based on the Ritz method. Two values of the thickness ratio h/b and different values of the Winkler foundation parameter $\overline{k}_w$ are considered. The results in this table illustrate the notable accuracy of the proposed method. Once again, the frequencies increase with the increase in the mode numbers, the thickness ratio h/b, and the Winkler foundation parameter. However, the frequencies decrease as the thickness ratio increases.

In the following, we will present some illustrative figures to demonstrate the effect of different parameters of the natural frequencies $\overline{\omega}_{11} = \omega_{11} h\sqrt{\rho/E_2}$. The laminated plates in all figures are made of Material I. Figures 2 and 3 display the 3D fundamental frequencies $\overline{\omega}_{11}$ of $(0°/90°/\ldots)$ symmetric square and rectangular ($a/b = 2$) plates vs Winkler's $\overline{\kappa}_w$, and Pasternak's $\overline{\kappa}_s$ parameters ($a/h = 5$). The frequencies increase as the number of layers increases. Also, the frequencies rapidly increase with the increase in Winkler's $\overline{\kappa}_w$ foundation parameter. The frequencies for the rectangular plates are greater than the corresponding ones for the square plates.

Figures 4 and 5 display the 3D natural frequencies $\overline{\omega}_{22}$ of $(0°/90°/\ldots)$ symmetric square and rectangular ($a/b = 2$) plates vs Winkler's $\overline{\kappa}_w$, and Pasternak's $\overline{\kappa}_s$ parameters ($a/h = 5$). The frequencies increase as the number of layers increases. Also, the frequencies for square plates rapidly increase with the increase in the foundation parameters (Fig. 4). While Fig. 5 shows that the frequencies for rectangular plates rapidly increase with the increase in Pasternak's $\overline{\kappa}_s$ parameter. Once again, the frequencies for the rectangular plates are greater than the corresponding ones for the square plates.

Figures 6 and 7 display the 3D fundamental $\overline{\omega}_{11}$ and natural $\overline{\omega}_{12}$, $\overline{\omega}_{22}$ frequencies of a four-layer $(0°/90°/90°/0°)$ square and rectangular ($a/b = 2$) sandwich plates vs. Winkler's $\overline{\kappa}_w$, and Pasternak's $\overline{\kappa}_s$ parameters ($a/h = 5$). The frequencies increase as the mode number increases. For square sandwich plates (Fig. 6), the frequencies $\overline{\omega}_{11}$ and $\overline{\omega}_{12}$ rapidly increase with the increase in Winkler's $\overline{\kappa}_w$ foundation parameter. While frequencies $\overline{\omega}_{22}$ rapidly increase with the increase in both foundation parameters. For rectangular sandwich plates (Fig. 7), the fundamental frequencies $\overline{\omega}_{11}$ rapidly increase with the increase in Winkler's $\overline{\kappa}_w$ foundation parameter. While the natural frequencies and $\overline{\omega}_{12}$ and $\overline{\omega}_{22}$ rapidly increase with the increase in Pasternak's $\overline{\kappa}_s$ foundation parameter.

Figure 8 shows the fundamental frequencies of $(0°/90°/\ldots)$ symmetric rectangular plates resting on an

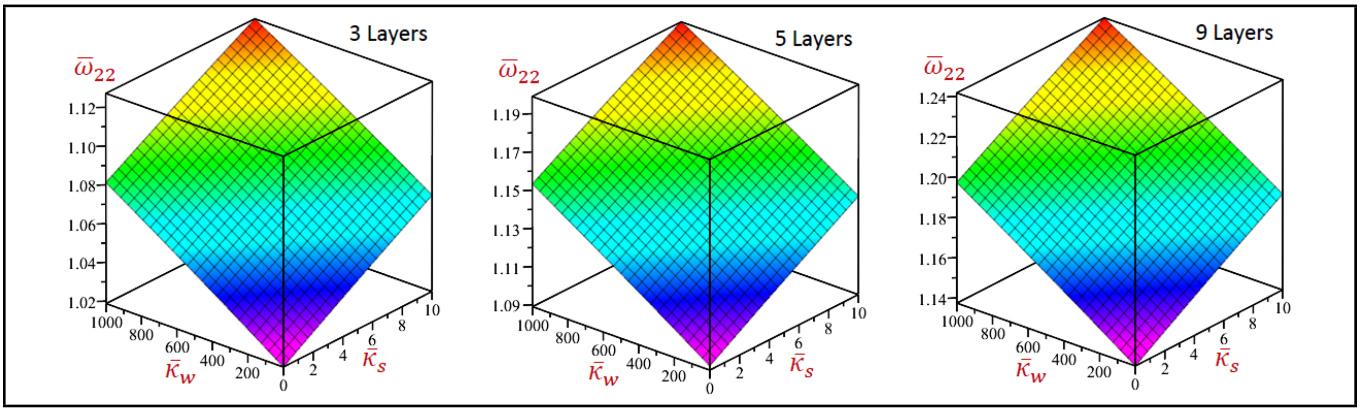

Figure 4. The 3D natural frequencies $\overline{\omega}_{22}$ of $(0°/90°/0°/\ldots)$ symmetric square plates vs. Winkler's $\overline{\kappa}_w$, and Pasternak's $\overline{\kappa}_s$ parameters $(a/h = 5)$.

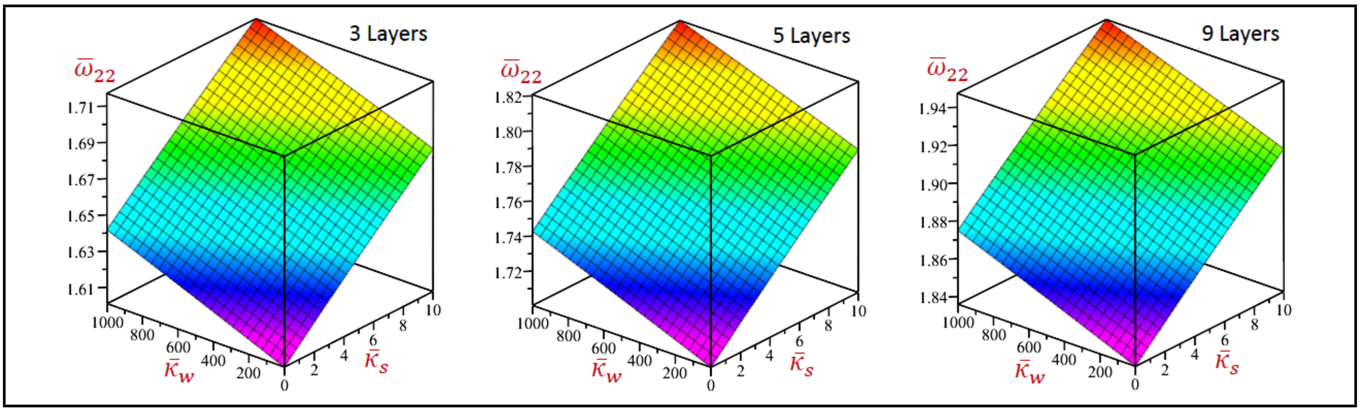

Figure 5. The 3D natural frequencies $\overline{\omega}_{22}$ of $(0°/90°/0°/\ldots)$ symmetric rectangular plates vs. Winkler's $\overline{\kappa}_w$, and Pasternak's $\overline{\kappa}_s$ parameters $(a/h = 5, a/b = 2)$.

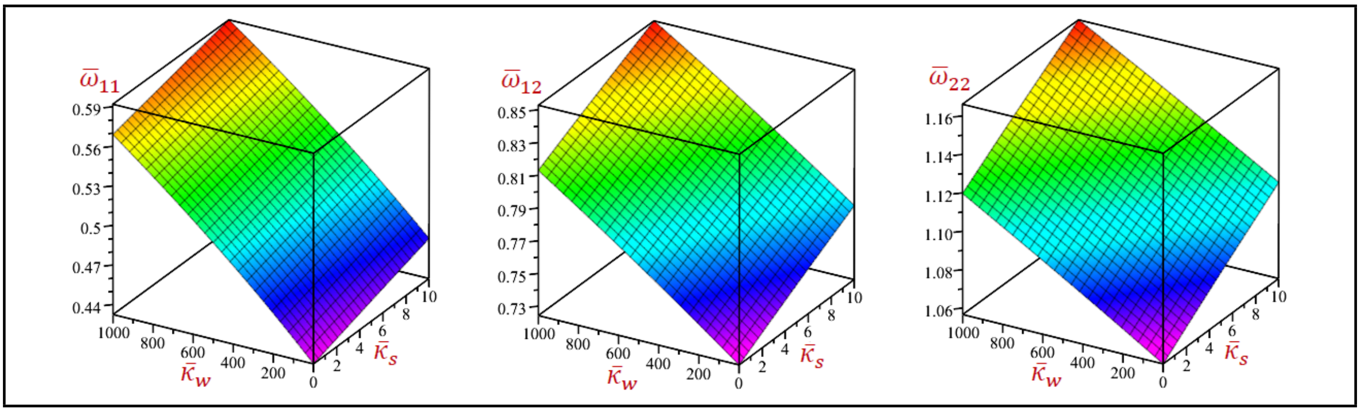

Figure 6. The 3D natural frequencies of a $(0°/90°/90°/0°)$ symmetric square plate vs. Winkler's $\overline{\kappa}_w$, and Pasternak's $\overline{\kappa}_s$ parameters $(a/h = 5)$.

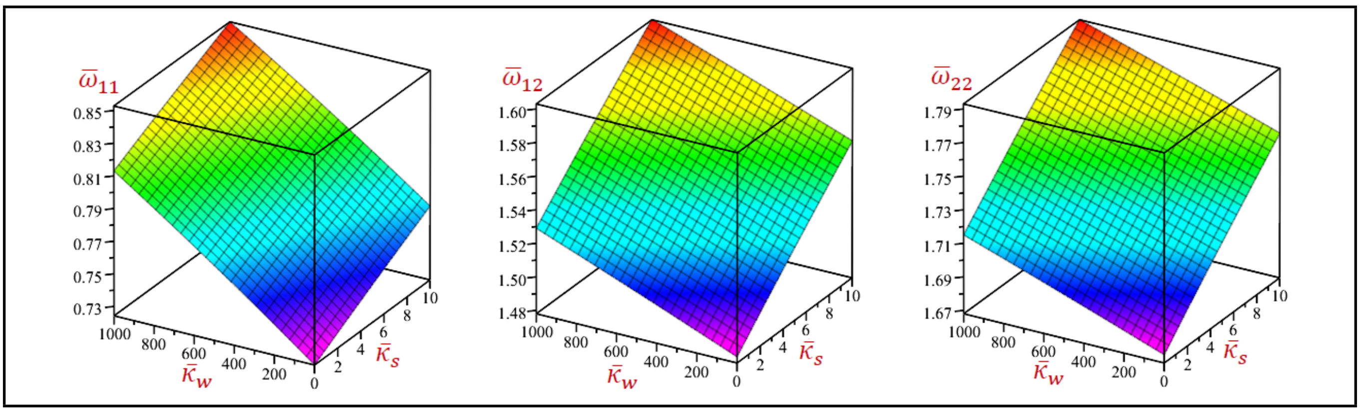

Figure 7. The 3D natural frequencies of a $(0°/90°/90°/0°)$ symmetric rectangular plate vs. Winkler's $\overline{\kappa}_w$, and Pasternak's $\overline{\kappa}_s$ parameters $(a/h = 5, a/b = 2)$.

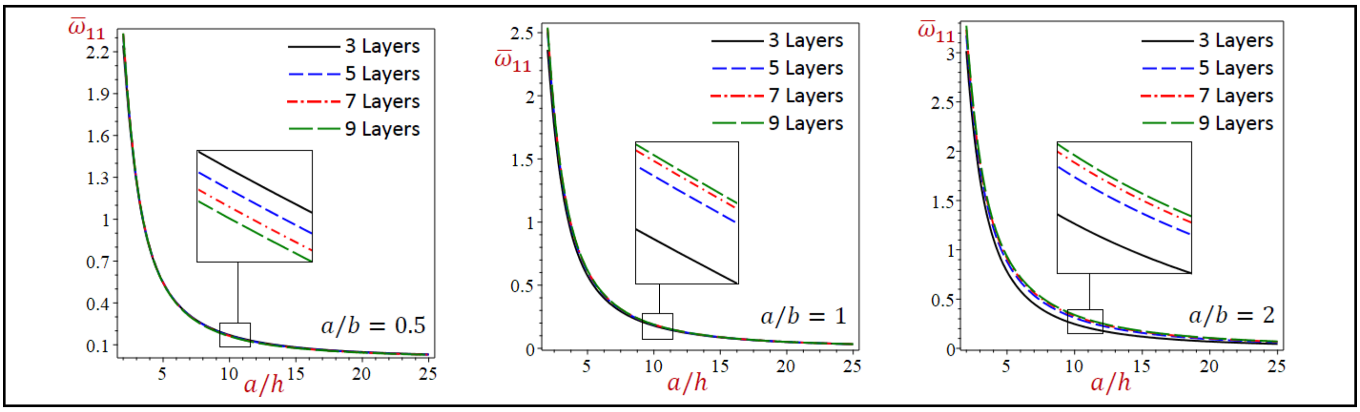

Figure 8. The fundamental frequencies of $(0°/90°/\ldots)$ symmetric rectangular plates vs. side-to-thickness ratio ($\overline{\kappa}_s = 10, \overline{\kappa}_w = 10^3$).

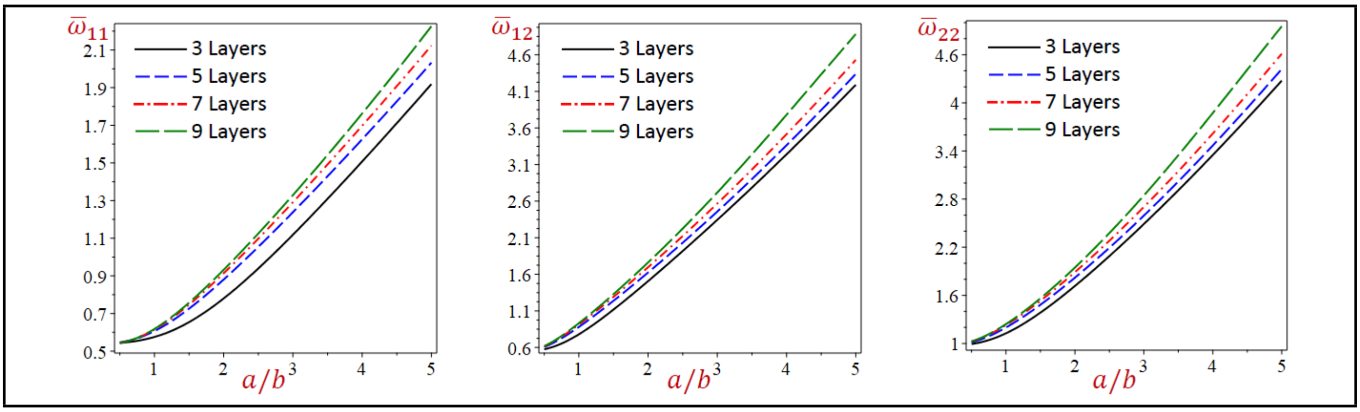

Figure 9. The natural frequencies of $(0°/90°/\ldots)$ symmetric rectangular plates vs. aspect ratio ($\overline{\kappa}_s = 10, \overline{\kappa}_w = 10^3, a/h = 5$).

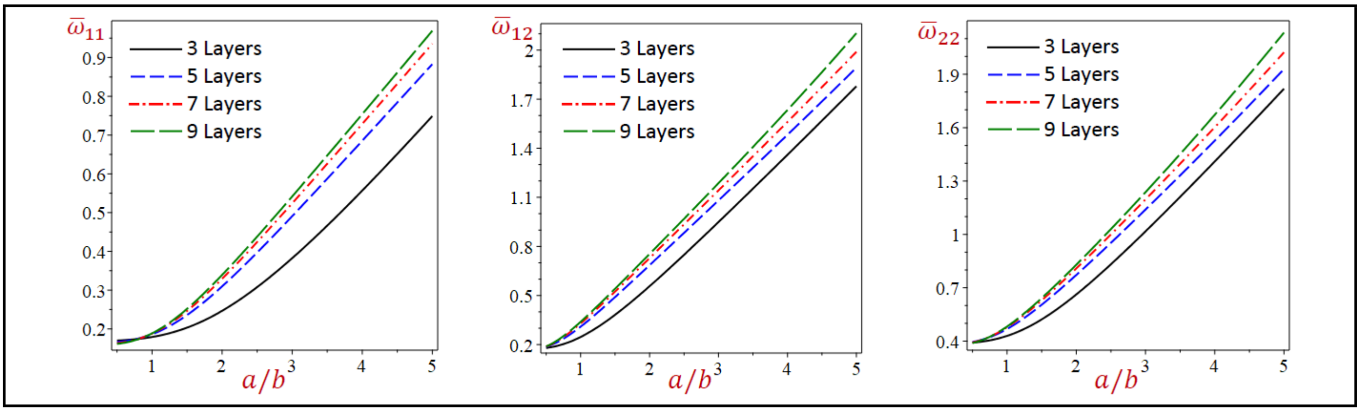

Figure 10. The natural frequencies of $(0°/90°/\ldots)$ symmetric rectangular plates vs. aspect ratio ($\overline{\kappa}_s = 10, \overline{\kappa}_w = 10^3, a/h = 10$).

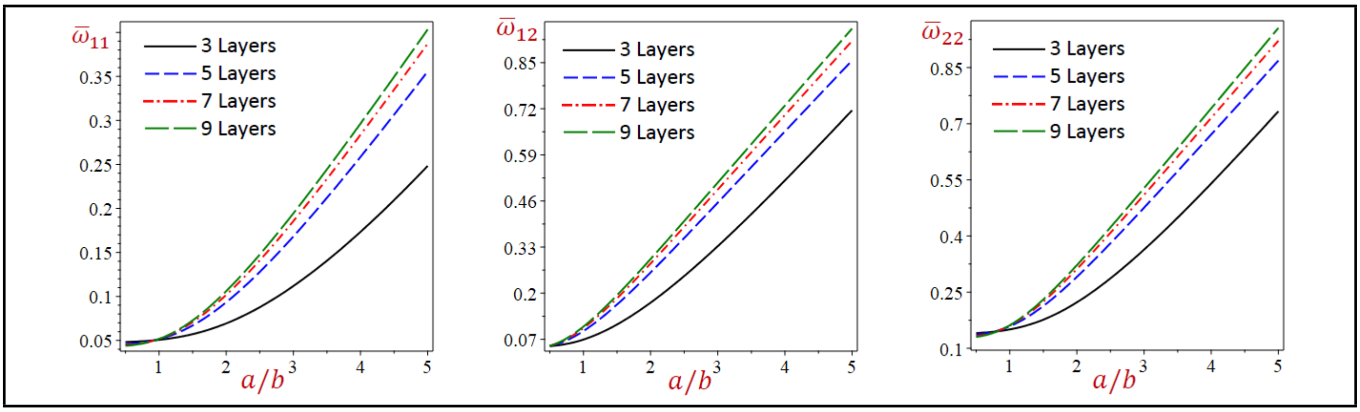

Figure 11. The natural frequencies of $(0°/90°/\ldots)$ symmetric rectangular plates vs. aspect ratio ($\overline{\kappa}_s = 10, \overline{\kappa}_w = 10^3, a/h = 20$).

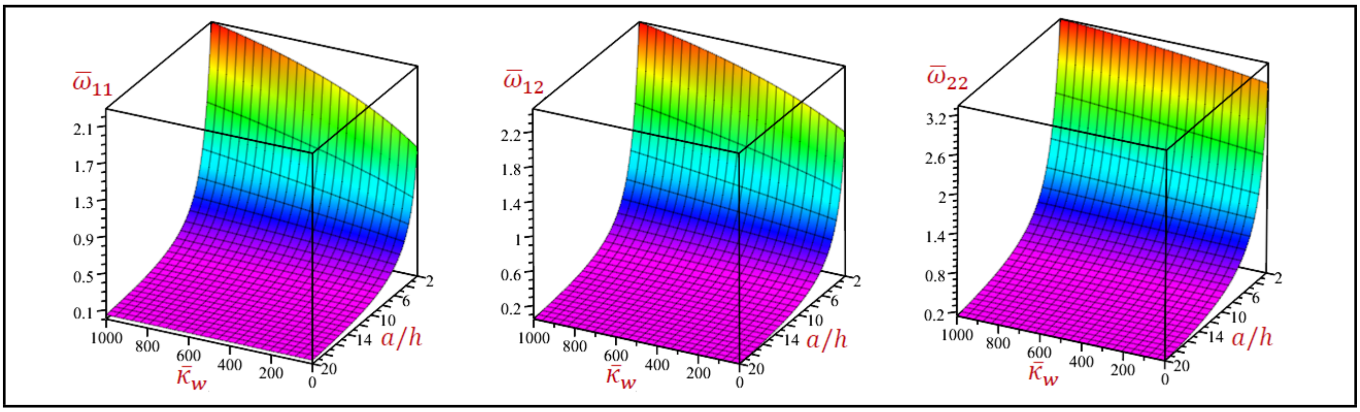

Figure 12. The 3D natural frequencies of a $(0^\circ/90^\circ/90^\circ/0^\circ)$ symmetric rectangular plate vs. Winkler's parameter $\overline{\kappa}_w$ and side-to-thickness ratio $a/$h ($\overline{\kappa}_s = 10$, $a/b = 0.5$).

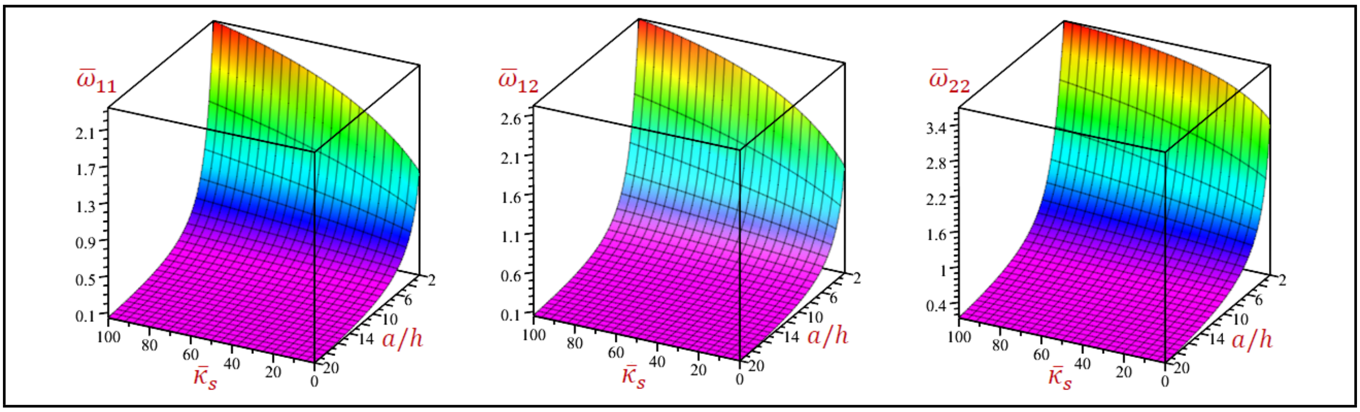

Figure 13. The 3D natural frequencies of a $(0^\circ/90^\circ/90^\circ/0^\circ)$ symmetric rectangular plate vs. Pasternak's parameter $\overline{\kappa}_s$ and side-to-thickness ratio a/h ($\overline{\kappa}_w = 10$, $a/b = 0.5$).

elastic foundation versus the side-to-thickness ratio a/h ($\overline{\kappa}_s = 10$, $\overline{\kappa}_w = 10^3$). The fundamental frequencies decrease as a/h increases. Also, the frequencies increase as the number of layers decreases when $b = 2a$. However, the frequencies increase as the number of layers increases when $b = a$ and $a = 2b$.

Figures 9–11 show the fundamental and natural frequencies of $(0^\circ/90^\circ/\ldots)$ symmetric rectangular plates resting on an elastic foundation versus the aspect ratio a/b for $a/h = 5$ in Fig. 9, for $a/h = 10$ in Fig. 10, and $a/h = 20$ in Fig. 11. The frequencies increase as the aspect ratio a/b, the number of layers, and the mode number increase. The frequencies for $a/h = 5$ in Fig. 9 are twice or more than the corresponding ones for $a/h = 10$ in Fig. 10 while the frequencies for $a/h = 10$ in Fig. 10 are twice or more than the corresponding ones for $a/h = 20$ in Fig. 11.

Figure 12 shows the 3D fundamental and natural frequencies of a four-layer $(0^\circ/90^\circ/90^\circ/0^\circ)$ symmetric rectangular sandwich plates versus Winkler's parameter $\overline{\kappa}_w$ and side-to-thickness ratio a/h ($\overline{\kappa}_s = 10$, $a/b = 0.5$). For a high value of $a/h = 20$, the frequencies are insensitive to the variation of Winkler's parameter $\overline{\kappa}_w$. However, for a small value of $a/h = 2$, the frequencies are slowly increasing as $\overline{\kappa}_w$ increases. Also, the frequencies increase as a/h decreases and this is irrespective of the value of Winkler's parameter $\overline{\kappa}_w$.

Figure 13 shows the 3D fundamental and natural frequencies of a four-layer $(0^\circ/90^\circ/90^\circ/0^\circ)$ symmetric rectangular sandwich plates versus Pasternak's parameter $\overline{\kappa}_s$ and side-to-thickness ratio a/h ($\overline{\kappa}_w = 10$, $a/b = 0.5$). For a high value $a/h = 20$, the frequencies are insensitive to the variation of Pasternak's parameter $\overline{\kappa}_s$. However, for a small value $a/h = 2$, the frequencies are slowly increasing as $\overline{\kappa}_s$ increases. Also, the frequencies increase as a/h decreases and this is irrespective of the value of Pasternak's parameter $\overline{\kappa}_s$.

Figure 14 shows the 3D fundamental and natural frequencies of a four-layer $(0^\circ/90^\circ/90^\circ/0^\circ)$ symmetric rectangular sandwich plates versus Winkler's parameter $\overline{\kappa}_w$ and aspect ratio a/b ($\overline{\kappa}_s = 10$, $a/h = 5$). For each value of the aspect ratio a/b, the frequencies are slightly increasing as Winkler's parameter $\overline{\kappa}_w$ increases. For higher values of the aspect ratio, especially when $a/b = 5$, the natural frequencies $\overline{\omega}_{12}$ and $\overline{\omega}_{22}$ are insensitive to the variation of Winkler's parameter $\overline{\kappa}_w$. However, all frequencies increase as a/b increases and this is irrespective of the value of Winkler's parameter $\overline{\kappa}_w$.

Figure 15 shows the 3D fundamental and natural frequencies of a four-layer $(0^\circ/90^\circ/90^\circ/0^\circ)$ symmetric rectangular sandwich plates versus Pasternak's parameter $\overline{\kappa}_s$ and aspect ratio a/b ($\overline{\kappa}_w = 10$, $a/h = 5$). It is interesting to note that all frequencies seen may be independent of the value of the aspect ratio a/b. However, for each value of the aspect ratio a/b, the frequencies are rapidly increasing as Pasternak's parameter $\overline{\kappa}_s$ increases. The values of the natural frequencies $\overline{\omega}_{22}$ maybe twice or more the values of the fundamental frequencies $\overline{\omega}_{11}$.

Finally, Figs. 16–18 show the 3D fundamental and natural frequencies of $(0^\circ/90^\circ/\ldots)$ anti-symmetric rectangular plates versus Winkler's $\overline{\kappa}_w$, and Pasternak's $\overline{\kappa}_s$ parameters ($a/h = 5$, $a/b = 0.5$). All frequencies increase with the increase in the number of layers. The frequencies are slightly increas-

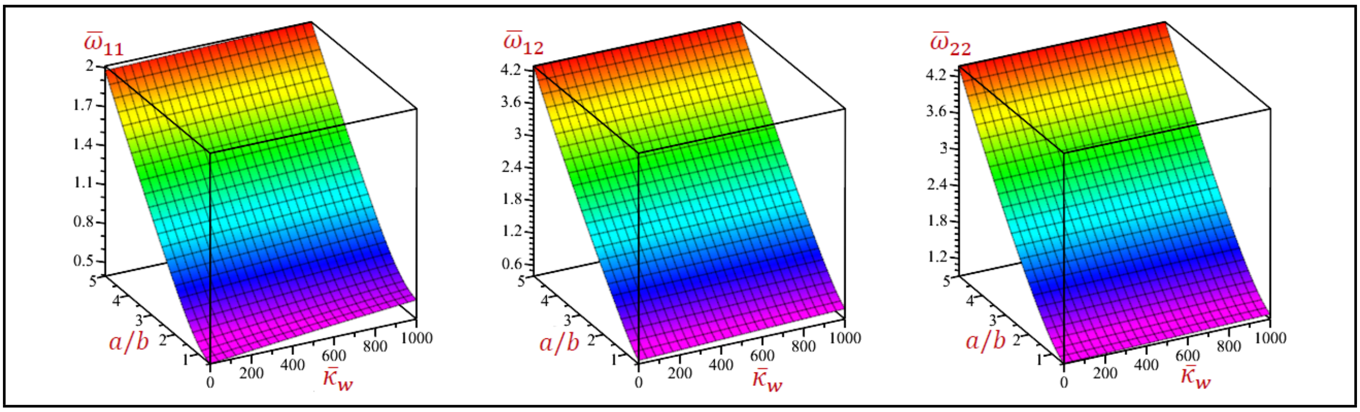

Figure 14. The 3D natural frequencies of a $(0°/90°/90°/0°)$ symmetric rectangular plate vs. Winkler's parameter $\overline{\kappa}_w$ and aspect ratio a/b ($\overline{\kappa}_s = 10$, $a/h = 5$).

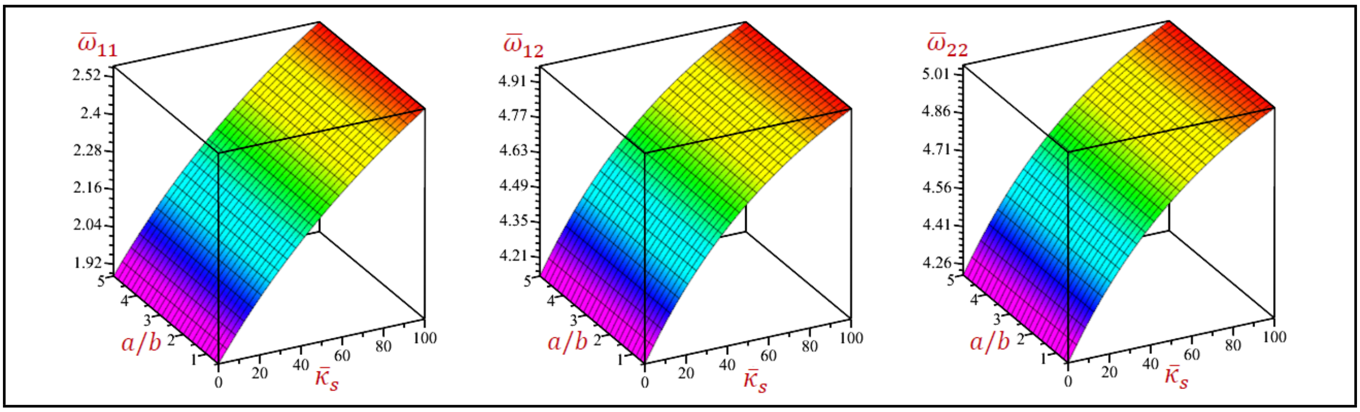

Figure 15. The 3D natural frequencies of a $(0°/90°/90°/0°)$ symmetric rectangular plate vs. Pasternak's parameter $\overline{\kappa}_s$ and aspect ratio a/b ($\overline{\kappa}_w = 10$, $a/h = 5$).

ing as Pasternak's $\overline{\kappa}_s$ parameter increases and rapidly increase as Winkler's $\overline{\kappa}_w$ parameter increases. The maximum frequencies occur at higher values of Winkler's $\overline{\kappa}_w$, and Pasternak's $\overline{\kappa}_s$ parameters. Also, the frequencies increase as the mode number increases. Irrespective of the number of layers, the natural frequencies $\overline{\omega}_{12}$ are greater than the corresponding fundamental frequencies $\overline{\omega}_{11}$. Also, the natural frequencies $\overline{\omega}_{22}$ maybe twice the values of the fundamental frequencies $\overline{\omega}_{11}$.

5. CONCLUSIONS

This paper proposed a quasi-3D refined plate theory for the vibrational frequencies of cross-ply laminated thick plates lying on elastic foundations. The accuracy and the reliability of the proposed analytical solution were evaluated and qualitatively verified. The findings reported in this study are summarized as follows:

- The theory accounts for the sinusoidal variation of transverse shear stresses and satisfies the free stress conditions on the upper and lower faces of the plate without utilizing any shear correction parameter;

- The accuracy of this theory is discussed across many examples for the vibration analyses of the studied plates with different values of thickness and aspect ratios as well as the foundation parameters;

- Different fundamental and natural frequencies predicted due to this theory are favorably compared with those that appeared in the literature;

- Most outcomes are tabulated and some new results are illustrated graphically for a wide range of foundation parameters, thickness, and aspect ratios; and,

- The illustrated frequencies may be used for future comparisons with other plate models.

ACKNOWLEDGEMENTS

This work was funded by the Deanship of Scientific Research (DSR) at King Abdulaziz University, Jeddah, under grant no. (130-76-D1438). The author, therefore, acknowledges with thanks DSR for technical and financial support.

REFERENCES

[1] Bhattacharya, A. P. Effects of edge restraints on the non-linear flexural vibrations of an imperfect cross-ply laminated plate resting on an elastic foundation, *Journal of Sound Vibration*, **105** (2), 265–274, (1986). https://doi.org/10.1016/0022-460X(86)90155-0

[2] Lal, A., Singh B. N., and Kumar, R. Natural frequency of laminated composite plate resting on an elastic foundation with uncertain system properties, *Structural Engineering and Mechanics*, **27** (2), 199–222, (2007). https://doi.org/10.12989/sem.2007.27.2.199

[3] Ayvaz, Y. and Oguzhan, C. B. Free vibration analysis of plates resting on elastic foundations using modified Vlasov

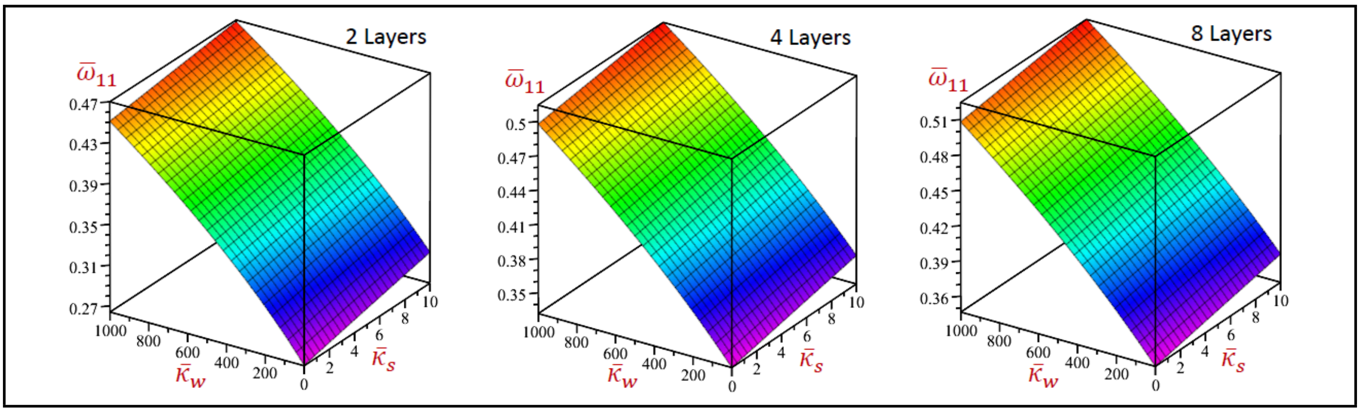

Figure 16. The 3D fundamental frequencies ϖ_{11} of $(0°/90°/\ldots)$ anti-symmetric rectangular plates vs. Winkler's $\overline{\kappa}_w$, and Pasternak's $\overline{\kappa}_s$ parameters ($a/h = 5$, $a/b = 0.5$).

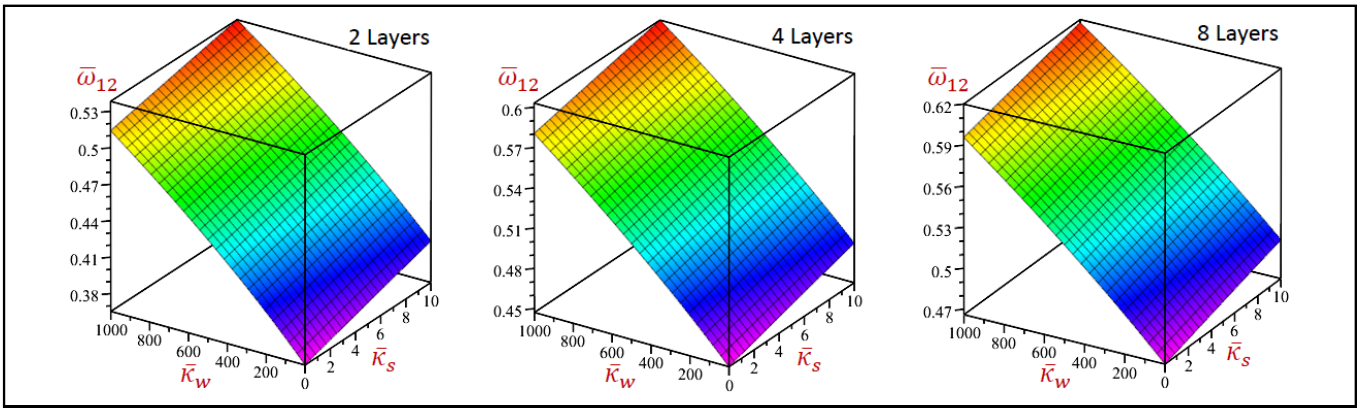

Figure 17. The 3D natural frequencies ϖ_{12} of $(0°/90°/\ldots)$ anti-symmetric rectangular plates vs. Winkler's $\overline{\kappa}_w$, and Pasternak's $\overline{\kappa}_s$ parameters ($a/h = 5$, $a/b = 0.5$).

model, *Structural Engineering and Mechanics*, **28** (6), 635–658, (2008). https://doi.org/10.12989/sem.2008.28.6.635

4 Pirbodaghi, T., Fesanghary, M., and Ahmadian, M. T. Non-linear vibration analysis of laminated composite plates resting on non-linear elastic foundations, *Journal of the Franklin Institute*, **348** (2), 353–368, (2011). https://doi.org/10.1016/j.jfranklin.2010.12.002

5 Akgöz, B. and Civalek, Ö. Nonlinear vibration analysis of laminated plates resting on nonlinear two-parameters elastic foundations, *Steel of Composite Structures*, **11** (5), 403–421, (2011). https://doi.org/10.12989/scs.2011.11.5.403

6 Nedri, K., El Meiche, N., and Tounsi, A. Free vibration analysis of laminated composite plates resting on elastic foundations by using a refined hyperbolic shear deformation theory, *Mechanics of Composite Materials*, **49** (6), 629–640, (2014). https://doi.org/10.1007/s11029-013-9379-6

7 Akgöz, B. and Civalek, Ö. Thermo-mechanical buckling behavior of functionally graded microbeams embedded in elastic medium, *International Journal of Engineering Science*, **85**, 90–104, (2014). https://doi.org/10.1016/j.ijengsci.2014.08.011

8 Mercan, K., Demir, Ç., and Civalek, Ö. Vibration analysis of FG cylindrical shells with power-law index using discrete singular convolution technique, *Curved Layered Structures*, **3** (1), 82–90, (2016). https://doi.org/10.1515/cls-2016-0007

9 Akgöz, B. and Civalek, Ö. Bending analysis of embedded carbon nanotubes resting on an elastic foundation using strain gradient theory, *Acta Astronautica*, **119**, 1–12, (2016). https://doi.org/10.1016/j.actaastro.2015.10.021

10 Haciyev, V. C., Sofiyev, A. H., and Kuruoglu N. Free bending vibration analysis of thin bidirectionally exponentially graded orthotropic rectangular plates resting on two-parameter elastic foundations, *Composite Structures*, **184**, 372–377, (2018). https://doi.org/10.1016/j.compstruct.2017.10.014

11 Haciyev, V. C., Sofiyev, A. H., and Kuruoglu, N. On the free vibration of orthotropic and inhomogeneous with spatial coordinates plates resting on the inhomogeneous viscoelastic foundation, *Mechanics of Advanced Materials and Structures*, **26** (10), 886–897, (2019). https://doi.org/10.1080/15376494.2018.1430271

12 Ozdemir, Y. I. Using fourth order element for free vibration parametric analysis of thick plates resting on elastic foundation, *Structural Engineering and Mechanics*, **65** (3), 213–222, (2018). https://doi.org/10.12989/sem.2018.65.3.213

13 Rahmani, A., Faroughi, S., and Friswell, M. I. Vibration analysis for anti-symmetric laminated composite plates resting on visco-elastic foundation with temperature effects, *Applied Mathematical Modelling*, **94**, 421–445, (2021). https://doi.org/10.1016/j.apm.2021.01.026

14 Mahmure, A., Tornabene, F., Dimitri, R., and Kuruoglu, N. Free vibration of thin-walled composite

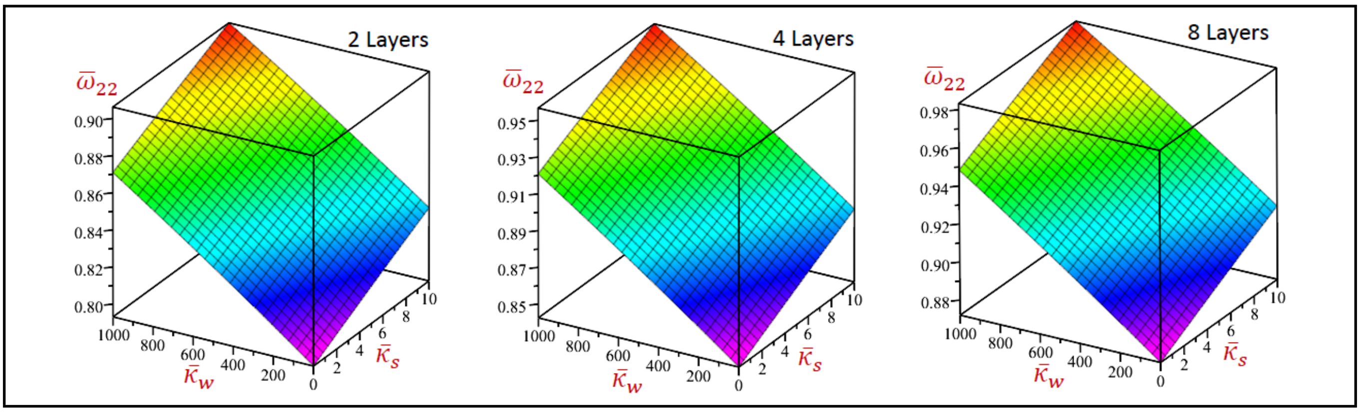

Figure 18. The 3D natural frequencies $\overline{\omega}_{22}$ of $(0°/90°/\ldots)$ anti-symmetric rectangular plates vs. Winkler's $\overline{\kappa}_w$, and Pasternak's $\overline{\kappa}_s$ parameters ($a/h = 5$, $a/b = 0.5$).

shell structures reinforced with uniform and linear carbon nanotubes: effect of the elastic foundation and nonlinearity, *Nanomaterials*, **11** (8), 2090, (2021). https://doi.org/10.3390/nano11082090

[15] Gohari, S., Mozafari, F., Moslemi, N., Mouloodi, S., Sharifi, S., Rahmanpanah, H., and Burvill, C. Analytical solution of the electro-mechanical flexural coupling between piezoelectric actuators and flexible-spring boundary structure in smart composite plates, *Archives of Civil and Mechanical Engineering*, **21**, 33, (2021). https://doi.org/10.1007/s43452-021-00180-z

[16] Gohari, S., Mouloodi, S., Mozafari, F., Alebrahim, R., Moslemi, N., Burvill, C., and Albarody, T. M. B. A new analytical solution for elastic flexure of thick multi-layered composite hybrid plates resting on Winkler elastic foundation in air and water, *Ocean Engineering*, **235**, 109372, (2021). https://doi.org/10.1016/j.oceaneng.2021.109372

[17] Yang, C., Huang, B., Guo, Y., and Wang, J. Characterization of delamination effects on free vibration and impact response of composite plates resting on visco-Pasternak foundations, *International Journal of Mechanical Sciences*, **212**, 106833, (2021). https://doi.org/10.1016/j.ijmecsci.2021.106833

[18] Guo, Y., Huang, B., Hua, L., Chen, J., and Wang, J. Modeling of partially delaminated composite plates resting on two-parameter elastic foundation with improved layerwise theory, *Mechanics of Advanced Materials and Structures*, In press, (2022). https://doi.org/10.1080/15376494.2022.2044571

[19] Huang, B., Wang, J., and Guo, Y. Investigation of delamination effect on nonlinear vibration behaviors of a composite plate resting on nonlinear elastic foundation, *Composite Structures*, **280**, 114897, (2022). https://doi.org/10.1016/j.compstruct.2021.114897

[20] Avey, M., Fantuzzi, N., Sofiyev, A. H., and Kuruoglu, N. Influences of elastic foundations on the nonlinear free vibration of composite shells containing carbon nanotubes within shear deformation theory, *Composite Structures*, **286**, 115288, (2022). https://doi.org/10.1016/j.compstruct.2022.115288

[21] Reddy, J. N. A simple higher-order theory for laminated composite plates, *Journal of Applied Mechanics*, **51** (4), 745–752, (1984). https://doi.org/10.1115/1.3167719

[22] Touratier, M. An efficient standard plate theory, *International Journal of Engineering Science*, **29** (8), 901–916, (1991). https://doi.org/10.1016/0020-7225(91)90165-Y

[23] Zenkour, A. M. Benchmark trigonometric and 3-D elasticity solutions for an exponentially graded thick rectangular plate, *Archive of Applied Mechanics*, **77** (4), 197–214, (2007). https://doi.org/10.1007/s00419-006-0084-y

[24] Zenkour, A. M. Quasi-3D refined theory for functionally graded porous plates: Displacements and stresses, *Physical Mesomechanics*, **23** (1), 39-–53, (2020). https://doi.org/10.1134/S1029959920010051

[25] Soldatos, K. P. A transverse shear deformation theory for homogeneous monoclinic plates, *Acta Mechanica*, **94**, 195–220, (1992). https://doi.org/10.1007/BF01176650

[26] Karama, M., Afaq, K. S., and Mistou, S. A new theory for laminated composite plates, *Journal of Materials Design and Applications*, **223** (2), 53–62, (2009). https://doi.org/10.1243/14644207JMDA189

[27] Noor, A. K. Free vibration of multilayered composite plates, *AIAA Journal*, **11**, 1038–1039, (1973). https://doi.org/10.2514/3.6868

[28] Putcha, N. S. and Reddy, J.N. Stability and natural vibration analysis of laminated plates by using a mixed element based on a refined plate theory, *Journal of Sound and Vibration*, **104** (2), 285–300, (1986). https://doi.org/10.1016/0022-460X(86)90269-5

[29] Khdeir, A. A. Free vibration and buckling of symmetric cross-ply laminated plates by an exact method, *Journal Sound and Vibration*, **126** (3), 447–461, (1988). https://doi.org/10.1016/0022-460X(88)90223-4

[30] Khdeir, A. A. and Librescu, L. Analysis of symmetric cross-ply elastic plates using a higher-order theory: Part II—Buckling and free vibration, *Composite Structures*, **9** (4), 259–277, (1988). https://doi.org/10.1016/0263-8223(88)90048-7

[31] Phan, N. D. and Reddy, J. N. Analysis of laminated composite plates using a higher-order shear deformation theory, *International Journal of Numerical Methods in Engineering*, **21**, 2201–2219, (1985). https://doi.org/10.1002/nme.1620211207

[32] Wu, C.-P. and Chen, W.-Y. Vibration and stability of laminated plates based on a local high order theory, *Journal of Sound and Vibration*, **177** (4), 503–520, (1994). https://doi.org/10.1006/jsvi.1994.1448

[33] Senthilnarthan, N. R., Lim, S. P., Lee, K. H., and Chow, S. T. Vibration of laminated orthotropic plates using a simplified higher order deformation theory, *Composite Structures*, **10** (3), 211–229, (1988). https://doi.org/10.1016/0263-8223(88)90020-7

[34] Reddy, J. N. and Phan, N. D. Stability and vibration of isotropic, orthotropic and laminated plates according to a high order shear deformation theory, *Journal of Sound and Vibration*, **98**, 157–170, (1985). https://doi.org/10.1016/0022-460X(85)90383-9

[35] Reddy, J. N. and Khdeir, A. A. Buckling and vibration of laminated composite plates using various plate theories, *AIAA Journal*, **27** (12), 1808–1817, (1989). https://doi.org/10.2514/3.10338

[36] Noor, A. K. and Burton, W. S. Stress and free vibration analyses of multilayered composite plates, *Composite Structures*, **11** (3), 183–204, (1989). https://doi.org/10.1016/0263-8223(89)90058-5

[37] Kant, T. and Kommineni, J. R. Large amplitude free vibration analysis of cross-ply composite and sandwich laminates with a refined theory and C0 finite elements, *Computers and Structures*, **50** (1), 123–134, (1994). https://doi.org/10.1016/0045-7949(94)90443-X

[38] Matsunaga, H. Vibration of cross-ply laminated composite plates, *Structural Engineering, Mechanics and Computation*, **1**, 541–548, (2001). https://doi.org/10.1016/B978-008043948-8/50057-6

[39] Lam, K. Y., Wang, C. M., and He, X. Q. Canonical exact solutions for Levy-plates on two parameter foundation using Green's functions, *Engineering Structures*, **22** (4), 364–378, (2000). https://doi.org/10.1016/S0141-0296(98)00116-3

[40] Hasani Baferani, A. and Saidi, A. R. Effects of in-plane loads on vibration of laminated thick rectangular plates resting on elastic foundation: An exact analytical approach, *European Journal of Mechanics—A/Solids*, **42**, 299–314, (2013). https://doi.org/10.1016/j.euromechsol.2013.07.001

[41] Akhavan, H., Hosseini-Hashemi, S., Damavandi Taher, H. R., Alibeigloo, A., and Vahabi, S. Exact solutions for rectangular Mindlin plates under in-plane loads resting on Pasternak elastic foundation. Part II: Frequency analysis, *Computational Materials Science*, **44** (3), 951–961, (2009). https://doi.org/10.1016/j.commatsci.2008.07.001

[42] Thai, H-T., Park, M., and Choi, D-H. A simple refined theory for bending, buckling, and vibration of thick plates resting on elastic foundation, *International Journal of Mechanical Sciences*, **73**, 40–52, (2013). https://doi.org/10.1016/j.ijmecsci.2013.03.017

[43] Dehghan, M. and Baradaran, G. H. Buckling and free vibration analysis of thick rectangular plates resting on elastic foundation using mixed finite element and differential quadrature method, *Applied Mathematics and Computation*, **218** (6), 2772–2784, (2011). https://doi.org/10.1016/j.amc.2011.08.020

[44] Zhou, D., Cheung, Y. K., Lo, S. H., and Au, F. T. K. Three-dimensional vibration analysis of rectangular thick plates on Pasternak foundation, *International Journal of Numerical Methods in Engineering*, **59** (10), 1313–1334, (2004). https://doi.org/10.1002/nme.915

[45] Xiang, Y., Wang, C. M., and Kitipornchai, S. Exact vibration solution for initially stressed Mindlin plates on Pasternak foundations, *International Journal of Mechanical Sciences*, **36** (4), 311–316, (1994). https://doi.org/10.1016/0020-7403(94)90037-X

[46] Leissa, A. W. The free vibration of rectangular plates, *Journal of Sound and Vibration*, **31** (3), 257–293, (1973). https://doi.org/10.1016/S0022-460X(73)80371-2

[47] Matsunaga, H. Vibration and stability of thick plates on elastic foundations, *Journal of Engineering Mechanics*, **126** (1), 27–34, (2000). https://doi.org/10.1061/(ASCE)0733-9399